Bacterial analogs of plant piperidine alkaloids mediate microbial interactions in a rhizosphere model system

Gabriel L. Lozano[1,2], Hyun Bong Park[3,4], Juan I. Bravo[1,2], Eric A. Armstrong[5], John M. Denu[5], Eric V. Stabb[6], Nichole A. Broderick[7], Jason M. Crawford[3,4,8*], Jo Handelsman[1,2*]

[1]Wisconsin Institute for Discovery and Department of Plant Pathology, University of Wisconsin-Madison

[2]Department of Molecular, Cellular and Developmental Biology, Yale University

[3]Department of Chemistry, Yale University

[4]Chemical Biology Institute, Yale University

[5]Wisconsin Institute for Discovery and Department of Biomolecular Chemistry, University of Wisconsin-Madison

[6]Department of Microbiology, University of Georgia

[7]Department of Molecular and Cell Biology, University of Connecticut

[8]Department of Microbial Pathogenesis, Yale School of Medicine

* Co-correspondence: jason.crawford@yale.edu, jo.handelsman@wisc.edu

ABSTRACT

Plants expend significant resources to select and maintain rhizosphere communities that benefit their growth and protect them from pathogens. A better understanding of assembly and function of rhizosphere microbial communities will provide new avenues for improving crop production. Secretion of antibiotics is one means by which bacteria interact with neighboring microbes and sometimes change community composition. In our analysis of a taxonomically diverse consortium from the soybean rhizosphere, we found that *Pseudomonas koreensis* selectively inhibits growth of *Flavobacterium johnsoniae* and other members of the Bacteroidetes grown in soybean root exudate. A genetic screen in *P. koreensis* identified a previously uncharacterized biosynthetic gene cluster responsible for the inhibitory activity. The metabolites were isolated based on biological activity and were characterized using tandem-mass spectrometry, multidimensional NMR, and Mosher ester analysis, leading to the discovery of a new family of bacterial piperidine alkaloids, koreenceine A-D (**1**-**4**). Three of these metabolites are analogs of the plant alkaloid γ-coniceine. Comparative analysis of the koreenceine cluster with the γ-coniceine pathway revealed distinct polyketide synthase (PKS) routes to the defining piperidine scaffold, suggesting convergent evolution. Koreenceine-type pathways are widely distributed among *Pseudomonas* species, and koreenceine C was detected in another *Pseudomonas* sp. from a distantly related cluster. This work suggests that *Pseudomonas* and plants convergently evolved the ability to produce similar alkaloid metabolites that can mediate inter-bacterial competition in the rhizosphere.

47 **IMPORTANCE**

48 The microbiomes of plants are critical to host physiology and development. Microbes are
49 attracted to the rhizosphere due to massive secretion of plant photosynthates from roots.
50 Microorganisms that successfully join the rhizosphere community from bulk soil have access to
51 more abundant and diverse molecules, producing a highly competitive and selective
52 environment. In the rhizosphere, as in other microbiomes, there is little known about the genetic
53 basis for individual species' behaviors within the community. In this study, we characterized
54 competition between *Pseudomonas koreensis* and *Flavobacterium johnsoniae*, two common
55 rhizosphere inhabitants. We identified a widespread gene cluster in several *Pseudomonas* spp.,
56 which is necessary for the production of a novel family of piperidine alkaloids that are structural
57 analogs of plant alkaloids. We expand the known repertoire of antibiotics produced from
58 *Pseudomonas* in the rhizosphere and demonstrate the role of the metabolites in interactions with
59 other bacteria of the rhizosphere.

60

61 **KEYWORDS**

62 *Flavobacterium johnsoniae*, *Pseudomonas koreensis*, antibiotics, bacterial competition,
63 convergent evolution

64

INTRODUCTION

Plants were long thought to be defined by their genes and environments. It has recently become apparent that plants are also shaped by their microbiomes — the communities of microorganisms that live on, around, and inside them (1). Microbiomes modify many environments, including humans, animals, oceans, soils, and hot springs. Comprehensive investigations of the interactions between microbiomes and their environments, as well as the interactions within microbiomes that contribute to their function and stability, are important to understand diverse niches on Earth, including those associated with plants.

The rhizosphere comprises plant root surfaces and their surrounding soil microenvironments. Bacteria are attracted to this environments by the massive amount of plant photosynthate, in the form of sugars, organic acids, and amino acids, which is secreted from roots (2). Bacteria that colonize the rhizosphere play an essential role in plant growth, and resistance to pathogens. For example, some members secrete plant-like hormones, such as indole acetic acid, gibberellic acid, cytokinin and abscisic acid, that promote plant growth (3), whereas others suppress plant diseases by secreting diverse compounds such as zwittermicin A, 2,4-diacetylphloroglucinol, and pyoluteorin (4). Thus, bacterial rhizosphere communities represent a rich reservoir of bioactive metabolites.

Use of bacteria for biological control of plant disease has been pursued for decades, but foreign microorganisms typically do not persist in native rhizosphere communities (5). Nutrient abundance, host availability, and microbial interactions define indigenous microbial community structures and limit colonization by invading bacteria. To engineer plant microbiomes to improve agricultural systems, a better understanding of the inter-bacterial interactions that dominate the rhizosphere is needed.

We developed ***t***he ***h***itchhikers ***o***f the ***r***hizosphere (THOR), a model system to examine the molecular interactions among core bacterial members of the rhizosphere (6). This model system is composed of *Bacillus cereus*, *Flavobacterium johnsoniae*, and *Pseudomonas koreensis,* which belong to three dominant phyla within the rhizosphere — Firmicutes, Bacteroidetes, and Proteobacteria, respectively. The three members display both competitive and cooperative interactions. For example, *P. koreensis* inhibits growth of *F. johnsoniae,* but not in the presence of *B. cereus*. Inhibition was only observed when bacteria were grown in soybean root exudate and is specific for Bacteroidetes, since this phylum was the only one inhibited by *P. koreensis* from a collection of taxonomically diverse rhizosphere bacteria (6). In this study, we characterized the genetic and molecular mechanisms by which *P. koreensis* inhibits *F. johnsoniae*. We determined that a new family of bacterial piperidine alkaloids designated koreenceine A-D (**1**-**4**) are produced by an orphan polyketide synthase (PKS) pathway and mediate inhibition of members of the Bacteroidetes. Koreenceines A, B and C are structural analogs of the piperidine alkaloid γ-coniceine, produced by plants, and comparisons of the plant and bacterial biosynthetic pathways support a convergent evolutionary model.

RESULTS

Identification of an orphan *P. koreensis* pathway that is responsible for inhibiting growth of *F. johnsoniae*.

To identify the genes required for inhibition of *F. johnsoniae* by *P. koreensis* in root exudate, we screened 2,500 *P. koreensis* transposon mutants and identified sixteen that did not inhibit *F. johnsoniae* (Table 1). Two of these mutants mapped to an uncharacterized polyketide biosynthetic cluster containing 11 genes (Fig. 1). We deleted the entire gene cluster (Δ*kecA*-

111 *kec*F::*tet*), which abolished inhibitory activity against *F. johnsoniae* and other members of the
112 Bacteroidetes (Fig. S1). We designed this pathway as an orphan pathway since the encoded
113 natural product is unknown.

114 We developed a defined medium in which *P. koreensis* simulated the gene cluster-
115 dependent inhibitory activity against *F. johnsoniae* that was observed in root exudate (Fig. S2A).
116 Since we identified two independent mutants in the gene encoding a sensor histidine kinase,
117 *cbrA,* that was required for activity in root exudate (Table 1), we developed a defined medium
118 with the goal of activating the CbrAB system (7), which controls the utilization of alternative
119 carbon sources such as amino acids (8). Adding to defined medium the same mix of the amino
120 acids that was used to supplement root exudate induced *P. koreensis* to produce inhibitory
121 activity in the defined media (Fig. S2A). We tested 19 different individual amino acids, and
122 identified five, including aspartate, that induce inhibition of *F. johnsoniae* by *P. koreensis* (Fig.
123 S2B). A non-hydrolysable analog of aspartate, *N*-methyl-DL-aspartate (Asp*), did not stimulate
124 inhibitory activity, suggesting that catabolism of certain amino acids is required for activity (Fig.
125 S2B).
126
127 **Characterization of koreenceine metabolites from the orphan *P. koreensis* pathway.**
128 To characterize the inhibitory metabolites from the orphan *P. koreensis* pathway, we
129 compared the metabolomes of the wild-type strain and the non-inhibitory mutant grown in root
130 exudate. High-performance liquid chromatography/mass spectrometry (HPLC/MS)-based
131 analysis of the crude organic extracts led to the identification of peaks **1**-**4** that were completely
132 abolished in the mutant (Fig. 2). We carried out bioassay-guided preparative-scale HPLC
133 fractionation of the crude organic extract from a culture (5 L) of the wild-type *P. koreensis*

grown in defined medium. Peaks **1**, **2** and **4** were detected in fractions with antimicrobial activity against *F. johnsoniae*. High-resolution electrospray ionization-quadrupole-time-of-flight MS (HRESIQTOFMS) data of **1**-**4** revealed *m/z* 208.2067, 210.2224, 226.2171, and 278.1885, allowing us to calculate their molecular formulas as $C_{14}H_{26}N$, $C_{14}H_{28}N$, $C_{14}H_{27}NO$, and $C_{14}H_{29}ClNO_2$, respectively (Fig. 2, Fig. S3). We then proceeded with mass-directed isolation of these metabolites from a larger-scale culture in defined medium (12 L) of wild-type *P. koreensis* for NMR-based structural characterization.

The chemical structures of **1**-**4** were characterized through ^{1}H, 2D-NMR (gCOSY, gHSQC, and gHMBC), tandem MS, and Mosher ester analysis (Fig. 3, Fig. S3-7). Briefly, ^{1}H NMR spectra combined with gHSQC of **2** revealed the presence of six methylene groups including one downfield-shifted signal, six additional methylene, and one methyl group. Consecutive COSY cross-peaks from a triplet methyl H-15 (δ_H 1.86) to a methylene H-7 (δ_H 2.53) established a partial structure of a nonane-like hydrocarbon chain. Additional COSY correlations from a downfield-shifted methylene H-2 (δ_H 3.53) to a methylene H-5 (δ_H 2.72) also constructed a shorter 4×CH_2 chain. Key HMBC correlations from H-2, H-4 and H-7 to C-6 allowed us to construct the piperidine core in **2**. In contrast, the ^{1}H NMR spectrum of **4** showed the presence of a hydroxyl methine H-3 (δ_H 3.94), which was evident by COSY correlations with both methylene H-2 and H-4. The connectivity between H-1′ (δ_H 3.20) and H-4′ (δ_H 3.59) was established by additional COSY correlations, which was further supported to be a 4-chlorobutanamine-like partial structure by the presence of a mono-chlorine isotope distribution

pattern in the HRESIQTOFMS data. HMBC correlations from H-2 and H-1′ to an amide carbon C-1 unambiguously constructed the chemical structure of **4** to be *N*-(4-chlorobutyl)-3-hydroxydecanamide. Modified Mosher's reaction on the secondary alcohol at C-3 determined the absolute configuration of C-3 to be *R*, completing the absolute structure of **4**. The structure of metabolite **1**, an analog of **2**, was elucidated based on the ^{1}H and COSY NMR data that indicate the position of a *trans*-double bond between H-7and H-8. Finally, the chemical structure of **3** was deduced by comparative high-resolution tandem MS analyses with the closely related metabolites **1** and **2**.

Koreenceine structure-activity analysis.

We estimated the minimal inhibitory concentration (MIC) values of koreenceine B (**2**) and D (**4**), as 200 µg mL^{-1} for both metabolites against *F. johnsoniae*. We predicted that koreenceine D does not have a major role in the inhibitory activity, since koreenceine D (**4**) is present in root exudate cultures at levels 100-times less than koreenceine A (**1**), B (**2**), and C (**3**) (Fig. 2). We could not estimate an MIC for koreenceine A, as its levels diminish during the purification process. We synthesized koreenceine A and observed similar decomposition during purification (data not shown). Thus, we tested a semi-purified fraction of koreenceine B with a trace of koreenceine A, which had a stronger inhibitory effect than koreenceine B alone, (MIC 40 µg mL^{-1}). The significant increase in activity associated with trace amounts of koreenceine A suggests that this molecule is the major inhibitory molecule against *F. johnsionae* in the THOR rhizosphere model or is synergistic with koreenceine B.

Proposed biosynthesis of koreenceine metabolites.

The defining piperidine core of koreenceine metabolites A-C is observed in plant alkaloids such as γ-coniceine, a well characterized alkaloid from poison hemlock (*Conium maculatum*) (9). We analyzed the putative activities of the genes in the koreenceine biosynthetic cluster and identified genes with predicted or previously identified enzymatic activities needed for the production of γ-coniceine in plants (10-13) (Fig. 1, Fig. 4). We propose the following biosynthetic pathway of koreenceine A to C. The first five genes of the cluster, *kecABCDE*, encode a type II polyketide synthase system: *kecA* encodes an acyl carrier protein (ACP); *kecB* and *kecD* encode β-ketoacyl synthases (KSα); and *kecC* and *kecE* encode partial β-ketoacyl synthases with conserved thiolase domains (Chain-Length Factor-CLF or KSβ). This cluster may encode production machinery for two-heterodimer systems, KecB-KecC and KecD-KecE, for polyketide elongation over KecA, and might participate in the formation of a triketide intermediate derived from the condensation of two malonyl units and a decanoyl-, 3-hydroxy-decanoyl-, or a *trans*-2-decenoyl- unit. β-keto reductive modifications could be catalyzed by KecG and KecH reductases (Figure 4). Aminotransferase KecF is predicted to catalyze transamination of the aldehyde intermediate facilitating piperidine cyclization. KecF appears to be a multidomain protein with a predicted aminotransferase at the *N*-terminus and a general NAD(P)-binding domain (IPR036291) and a conserved protein domain COG5322 at the *C*-terminus. Interestingly, long-chain fatty acyl-ACP reductases from Cyanobacteria share these features and generate fatty aldehydes from the reduction of fatty acid intermediates bound to ACP (14). We predict that KecF reduces the ACP-polyketide intermediate to a polyketide aldehyde with the *C*-terminal domain, followed by transamination by the *N*-terminal domain. Finally, the amine intermediate could undergo a non-enzymatic cyclization as observed in γ-

199 coniceine (12). We predict that koreenceine D is derived from koreenceine C by an unidentified
200 halogenase reaction, as analogous metabolite sets have been detected in plants (Fig. S8) (15).
201 The last three genes, *kecIJK*, may participate in the translocation of the koreenceine alkaloids
202 outside of the cell. KecI and KecJ are hypothetical proteins predicted to localize in the membrane
203 and KecK has homology with membrane-bound drug transporters.
204
205 **Convergent evolution of pathways for production of γ-coniceine-like alkaloids in plants and**
206 ***P. koreensis*.**
207 The biosynthetic pathway for production of γ-coniceine is still under investigation, but
208 ^{14}C-feeding experiments in *C. maculatum* coupled with chemical degradation of the labeled
209 products suggest that γ-coniceine is not derived from an amino acid as are other plant alkaloids,
210 but rather it is derived from a polyketide chain produced by the condensation of acetate units
211 (10). Type III polyketide synthases common in plants are iterative homodimers that orchestrate
212 the acyl-CoA mediated priming, extension, and cyclization reactions for polyketide products
213 without the use of acyl carrier proteins (16). Recently, Hotti et al. found CPKS5, a non-chalcone
214 synthase/stilbene synthase (CHS/STS)-type III polyketide synthase expressed in tissues that
215 contain γ-coniceine (Fig. 4) (11). The pathway that we identified in *P. koreensis* predicted two
216 type II PKSs are involved in production of the polyketide intermediate (Fig. 1). Although the
217 pathway that we identified in *P. koreensis* produces compounds related to the plant alkaloids, the
218 PKSs from the plant and bacterial kingdoms share little similarity. We propose that convergent
219 evolution led to two different polyketide pathways for the production of γ-coniceine-like
220 metabolites in plants and bacteria.
221

Distribution of the koreenceine cluster.

Similar koreenceine-like clusters have previously been identified by functional screens for antimicrobial activities (17, 18); however, there are no reports of the metabolites produced. We identified 179 koreenceine-like clusters in genomes in NCBI (June 2018). The majority of these clusters are in *Pseudomonas* genomes, although we found some partial clusters lacking *kecIJK* in *Xenorhabdus* and *Streptomyces* spp. genomes (Fig. 5A). We used maximum-likelihood analysis of the amino acid sequence of the aminotransferase-reductase protein, KecF, as a representative of the koreenceine cluster for phylogenetic reconstruction. We observed four main clades that are each associated with a bacterial genus (Fig. 5A). Clades A and B, which contain 93% of the clusters, are found in *Pseudomonas* genomes. The koreenceine gene cluster identified in *P. koreensis* in this study belongs to Clade A; other Clade A clusters are located in the same genomic context in *P. koreensis* and *P. mandelii*, two closely related species in the *P. fluorescens* complex (19) (Fig. 5B). Clades C and D were found in *Streptomyces* and *Xenorhabdus* spp., respectively.

Clade A and the *P. koreensis* and *P. mandelii* genomes are phylogenetically parallel (Fig. 5C). We hypothesize that the gene cluster was acquired before *Pseudomonas fluorescens* complex diversification from a common ancestor of *P. koreensis* and *P. mandelii* and maintained in these *Pseudomonas spp.* by vertical transmission. In contrast, Clade B contains clusters present in *P. putida* and several species of the *P. fluorescens* complex, in which there is no conservation in the genome localization, and the clusters are frequently associated with elements that mediate horizontal gene transfer (Fig. 5B). This suggests different strategies to maintain koreenceine-type gene clusters in diverse *Pseudomonas* species.

Another *Pseudomonas* isolate (SWI36) was reported to inhibit *B. cereus*, and its activity was dependent on a koreenceine-type gene cluster from clade B (18), but we found that it did not inhibit *F. johnsoniae*. Under certain conditions, *P. koreensis* inhibited *B. cereus*, and the activity was dependent on the koreenceine cluster, suggesting a similarity with the SWI36 cluster (Fig. S9). Indeed, targeted metabolomic analysis of *Pseudomonas* sp. SWI36 cell-free culture detected koreenceine C (Fig. S10). These data suggest that different koreenceine-like gene clusters in *Pseudomonas* genomes have the capacity to synthesize koreenceine metabolites.

DISCUSSION

In this work, we aimed to understand the molecular basis for the growth inhibition of *F. johnsoniae* by *P. koreensis* on a route to elucidating interactions within the rhizosphere microbiome. We have shown that *P. koreensis* inhibits *F. johnsoniae* growth through the production and secretion of novel secondary metabolites, koreenceine A-D (**1**-**4**), which have structural similarity with the plant metabolite γ-coniceine. Based on the biosynthetic gene cluster identified through our genetic screen, we propose a type II polyketide biosynthetic pathway for these bacterial alkaloids. Traditionally type II polyketide synthases are iterative heterodimer systems. It is currently unclear if the two heterodimer systems present in the biosynthetic cluster act in a modular or iterative manner, but the number of putative β-ketoacyl synthase genes in the pathway is consistent with modular biosynthesis. Plants also use a polyketide pathway mediated by an iterative type III polyketide synthase, providing a new example of convergent evolution between these organisms for the synthesis of related alkaloids. The piperidine core of the koreenceine metabolites is found in well-known plant alkaloids, such as the active cytotoxin γ-coniceine from poison hemlock (*C. maculatum*). Thus, koreenceine alkaloids may play roles in

267 inter-bacterial and inter-Domain communication or inhibition that changes the rhizosphere
268 community structure.

269 Members of the genus *Pseudomonas* are ubiquitous in nature and thrive in soil, on plants,
270 and on moist surfaces. *P. koreensis* and other members of the *Pseudomonas fluorescens* complex
271 are often studied for their capacity to colonize the rhizosphere and protect plants from pathogens.
272 Previous research demonstrated that *P. fluorescens* suppresses plant disease through production
273 of phenazine-1-carboxylic acid (PCA), which targets the fungal pathogen *Gaeumannomyces*
274 *graminis* (20). *P. fluorescens* also produces a suite of antimicrobial compounds including 2,4-
275 diacetylphloroglucinol, pyoluteorin, pyrrolnitrin, lipopeptides, and hydrogen cyanide (4), and
276 members of the *P. fluorescens* complex also produce plant hormones, such as indole acetic acid
277 and gibberellic acid, that stimulate plant growth. In this paper, we expand the known repertoire
278 of metabolites from the *P. fluorescens* complex with koreenceine A-D. Unlike most of the *P.*
279 *fluorescens* metabolites that inhibit fungal pathogens, the koreenceines mediate interactions
280 between *P. koreensis* and diverse members of the Bacteroidetes, including *F. johnsoniae,* in a
281 family-specific manner (6). Competition between members of the *P. fluorescens* complex and
282 *Flavobacterium* spp. in natural settings has been reported; *in vivo* studies showed a selective
283 reduction of *Flavobacterium* spp. in the *Arabidopsis thaliana* rhizosphere when *Pseudomonas*
284 sp. CH267 was added to soil (21). Together, these results highlight the relevance of
285 characterizing bacterial-bacterial interactions in the rhizosphere.

286 We identified a gene cluster necessary for the production of the koreenceine metabolites.
287 Other koreenceine-like clusters have been predicted to mediate (22) and others are associated
288 with (17, 18) antagonistic activity against diverse microorganisms. Thirty-five percent of *P.*
289 *koreensis* and *P. mandelii* genomes in NCBI contain this cluster and there are at least 160

290 *Pseudomonas* genomes harboring a related cluster, indicating the widespread nature of this
291 cluster among *Pseudomonas* spp. Despite its ubiquity, structural characterization of the products
292 of the biosynthetic cluster have been identified slowly.

293 Bioinformatic analysis of the proposed activities of the genes in the cluster enabled us to
294 propose a biosynthetic pathway for the formation of a C_{14} polyketide with a piperidine-type ring
295 from a non-canonical type II PKS system (Fig. 2). In bacteria, piperidine-type rings could be
296 derived from lysine cyclization (23), as observed in plants, or by a two-step reduction-
297 transamination route of polyketide intermediates (24). We propose that the multidomain protein
298 KecF may direct both steps: reduction of the acyl-intermediate to generate the acyl-aldehyde and
299 transamination. This differs from the established route, in which the two activities are encoded in
300 different genes, and the reduction domain represents the terminal domain of a type I polyketide
301 synthase (Fig. 4) (24). We propose that β-ketoacyl synthase(s) incorporate trans-2-decenoyl-,
302 decanoyl-, or 3-hydroxy-decanoyl units to generate koreenceine A, B or C, respectively. It is
303 unclear if these acyl units are recruited as CoA esters from the β-oxidation pathway or as ACP
304 esters from fatty acid synthesis, although the *R* configuration in koreenceine D suggests substrate
305 sampling from the fatty acid synthesis pool (*i.e.*, fatty acyl-ACP).

306 Koreenceine A-C share structural features with γ-coniceine, the metabolite responsible
307 for the toxicity of the poison hemlock, a plant once used in death sentences, and the means by
308 which Socrates took his own life after receiving such a sentence (399 BC). The structural
309 similarity is the result of convergent evolution. Their functions may also be related—γ-coniceine
310 and its derivative make hemlock (*Conium maculatum*) toxic to animals (9) and *P. koreensis*
311 might protect plant roots with koreenceines. γ-coniceine is also considered a plant hormone (9,

312 25). Thus, future work will focus on characterizing the effect of koreenceine A-C on plant
313 development and protection.
314
315 **ACKNOWLEGMENTS**
316 We gratefully acknowledge Dr. Sailendharan Sudakaran for discussing phylogenetic
317 analysis. We thank Dr. Hans Wildschutte for *Pseudomonas* sp SWI36 and its mutant. This work
318 was supported by the Office of the Provost at Yale University, funding from the Wisconsin
319 Alumni Research Foundation through the University of Wisconsin–Madison Office of the Vice
320 Chancellor for Research and Graduate Education, and NSF grant MCB-1243671.
321
322 **MATERIALS AND METHODS**
323 **Bacterial strains and culture conditions.** *F. johnsoniae CI04*, *P. koreensis CI12*, *B.*
324 *cereus* UW85, *Pseudomonas* sp. SWI36, *Flavobacterium johnsoniae* CI64, *Chryseobacterium*
325 sp. CI02, *Chryseobacterium* sp. CI26, *Sphingobacterium* sp. CI01, and *Sphingobacterium* sp.
326 CI48 were propagated on 1/10th-strength tryptic soy agar and grown in liquid culture in ½-
327 strength tryptic soy broth (TSB) at 28°C with vigorous shaking.
328
329 **Production of root exudates and defined media.** Soybean seeds were surface sterilized
330 with 6% sodium hypochlorite for 10 min, washed with sterile deionized water, transferred to
331 water agar plates, and allowed to germinate for three days in the dark at 25^{o}C. Seedlings were
332 grown in a hydroponic system using modified Hoagland's plant growth solution (26), which was
333 collected after 10 days of plant growth in an environmental chamber (12-h photoperiod, 25°C),
334 filter sterilized and stored at -20°C until used as root exudate. A defined medium was based on

335 basal salt medium (1.77 g mL^{-1} Na_2HPO_4; 1.70 g mL^{-1} KH_2PO_4; 1.00 g mL^{-1} $(NH_4)_2SO_4$; 0.16 g
336 mL^{-1} $MgCl_2*6H_2O$; 5.00 g mL^{-1} $FeSO_4*7H_2O$). A carbon source (pyruvate, mannitol, or
337 glucose) was added to a final concentration of 4 mM. An amino acid mix of equal parts alanine,
338 aspartate, leucine, serine, threonine, and valine was added to the root exudate or the defined
339 minimal media at a final concentration of 6 mM. Individual amino acids and *N*-methyl-DL-
340 aspartate were also added to a final concentration of 6 mM.
341
342 ***P. koreensis* mutant library generation by transposon mutagenesis.** *P. koreensis* CI12
343 and *E. coli* S17-1λpir with pSAM_BT20 (27) with ampicillin (100 μg mL^{-1}) were first grown
344 individually for 16 h in LB at 28°C and 37°C, respectively, with agitation. Cells were washed
345 and resuspended in LB to an OD_{600} = 2.0. One volume of *E. coli* S17-1λpir with pSAM_BT20
346 was mixed with two volumes of *P. koreensis* CI12 were mixed. Cells were harvested (6000 × *g*,
347 6 min), resuspended in 100 μL of LB, and spotted on LBA. Plates were incubated at 28°C for 16
348 h. Each conjugation mixture was scraped off the plate, resuspended in 2.5 mL of LB, and 350-μL
349 aliquots were plated on LB containing gentamicin (50 μg mL^{-1}) and chloramphenicol (10 μg
350 mL^{-1}) to select for *P. koreensis* CI12 transconjugants. Plates were incubated for two days at
351 28°C.
352
353 **Genetic screen of *P. koreensis* mutants defective in inhibitory activity.** *P. koreensis*
354 CI12 mutants were grown for 16 h in 96-deepwell plates filled with ½-strength TSB, covered
355 with sterile breathable sealing films, and incubated at 28°C with agitation. For each plate, the
356 first well was inoculated with wild type *P. koreensis* CI12, and the last well was left without *P.*

357 *koreensis* CI12. *F. johnsoniae* CI04 was grown and washed as described above. Root exudate
358 was inoculated with ~10^7 *F. johnsoniae* CI04 cells per mL, and 200 µL aliquots were added to
359 each well of 96-well microplates. Next, two µL from each mutant *P. koreensis* CI12 culture was
360 transferred to the corresponding wells on the microplates, which were then covered by sealing
361 films and incubated at 28°C with slight agitation for two days. Five µL from each well were then
362 spotted on Casitone-yeast extract agar (CYE) (10 g L^{-1} casitone; 5 g L^{-1} yeast extract; 8 mM
363 MgSO4; 10 mM Tris buffer; 15 g L^{-1} agar) containing kanamycin (10 µg mL^{-1}) to select for *F.*
364 *johnsoniae*, and plates were incubated at 28°C for two days. Mutants that did not inhibit *F.*
365 *johnsoniae* were streaked on a second plate for further analysis. The loss of inhibitory activity of
366 candidate *P. koreensis* mutants was verified in a second co-culture, and mutant growth was then
367 compared to wild-type growth to rule out candidates that failed to inhibit *F. johnsoniae* due to
368 their own growth deficiency.
369
370 **Location transposons in *P. koreensis* mutants defective in *F. johnsoniae* inhibition.**
371 For each mutant, one mL of liquid culture grown for 16 h was harvested (6000 × *g*, 6 min), and
372 cells were resuspended in 400 mL of TE (10 µM TrisHCl pH 7.4; 1 µM EDTA pH 8.0). Samples
373 were boiled for 6 min, centrifuged (6000 × *g*, 6 min), and two µL of supernatant was used as a
374 template for DNA amplification. Transposon locations were determined by arbitrarily primed
375 PCR which consisted of a nested PCR using first-round primer GenPATseq1 and either AR1A or
376 AR1B and second-round primer GenPATseq2 and AR2 (Table 2). PCR products from the
377 second round were purified by gel extraction (QIAquick Gel Extraction Kit; QIAGEN) and then
378 sequenced using primer GenPATseq2.

Chromosomal deletion of the koreenceine gene cluster in *P. koreensis*. The koreenceine cluster was deleted by allelic exchange and replaced with a tetracycline resistant cassette. The *kecA-K* deletion cassette was constructed by a modified version of overlap extension (OE) PCR strategy. Fragments one kb upstream and one kb downstream of the *kecA-K* genes were amplified using primers mutSGCA_For/mutSGCA_Rev and mutSGCB_For/mutSGCB_Rev respectively (Table 2). The PCR products were cloned in pENTR/D-TOPO, generating pkecA-K_ENTR. Primers mutSGCA_Rev and mutSGCB_For were designed to include a KpnI site in their overlapping region to allow introduction of a resistance gene. A tetracycline resistance cassette was amplified from pACYC184 using primers TetA_For/TetA_Rev, which contain KpnI sites in the 5' region, and cloned into pENTR/D-TOPO to generate pTetA_ENTR. A *mob* element was amplified from pJN105 using primers pJN105Mob_For/pJN105Mob_Rev (Table 2), in which an AscI site in the 5' region was added, and cloned in pENTR/D-TOPO, generating pmob_ENTR. The tetracycline cassette was recovered from pTetA_ENTR using KpnI, and cloned between the region upstream and downstream of the pkecA-K_ENTR, and the *mob* element was recovered from pmob_ENTR using AscI, and cloned into an AscI site in the pENTR backbone, generating pkecA-K_TetA_mob_ENTR. Conjugation mixtures of *P. koreensis* CI12 and *E. coli* S17-1λpir carrying the pkecA-K_TetA_mob_ENTR vector were prepared following the procedure for the transposon mutant generation. Double recombinant *P. koreensis* CI12 transconjugants were selected by their ability to grow on tetracycline (10 μg mL^{-1}) and inability to grow on kanamycin (50 μg mL^{-1}). The *kekA-K* deletion mutant was confirmed by PCR using primers mutSGCA_For and mutSGCB_Rev. The *kekA-K* deletion mutant was further confirmed by evaluating growth of *F. johnsoniae*, and other members of the Bacteroidetes, in its presence.

General information for the analysis and identification of metabolites. ^{1}H and 2D-(gCOSY, gHSQC, and gHMBC) NMR spectra were obtained on an Agilent (USA) 600 MHz NMR spectrometer with a cold probe, and the chemical shifts were recorded as δ values (ppm) with methanol-d_4 as the standard NMR solvent. Materials were routinely analyzed on an Agilent 6120 single quadrupole liquid chromatography-mass spectrometry (LC/MS) system (Column: Phenomenex kinetex C_{18} column, 250 × 4.6 mm, 5 μm; Flow rate: 0.7 ml min^{-1}; Mobile phase composition: H_2O and acetonitrile (ACN) containing 0.1% trifluoroacetic acid (TFA); Method: 0-30 min, 10-100% ACN; hold for 5 min, 100% ACN; 1 min, 100-10% ACN). High-resolution electrospray ionization mass spectrometry (HR-ESIMS) data were obtained using an Agilent iFunnel 6550 Q-TOF (quadrupole-time-of-flight) mass spectrometer fitted with an electrospray ionization (ESI) source coupled to an Agilent (USA) 1290 Infinity high performance liquid chromatography (HPLC) system. Open column chromatography was carried out on a Waters Sep-Pak® Vac 35cc (10g) C_{18} column. Metabolite isolations were performed using an Agilent (USA) Prepstar HPLC system with an Agilent (USA) Polaris C_{18}-A 5 μm (21.2 × 250 mm) column, a Phenomenex (USA) Luna C_{18}(2) (100Å) 10 μm (10.0 × 250 mm) column, a Phenomenex (USA) Luna C_8(2) (100Å) 10 μm (10.0 × 250 mm) column, and an Agilent Polaris 5 Amide-C18 (250 × 10.0 mm) column.

Isolation of metabolites. *P. koreensis CI12* was grown in defined medium with pyruvate as carbon source and supplemented with the amino acid mix or 3mM of glutamate for 3 days. Crude extract was generated by liquid-liquid extraction using one volume of 2-butanol per one

volume of filter supernatant, and dried by rotary evaporation. The crude extracts (400 mg) from the 12-L culture supernatant were resuspended in water and methanol (1:1 ratio), adsorbed onto Celite® 110, and dried by rotary evaporation. The resulting powdery materials were loaded on the Waters Sep-Pak® Vac 35cc (10g) C_{18} cartridge, and the metabolites were separated by solvent fractionation, eluting with a step gradient from 20-100% aqueous methanol to yield five sub-fractions (20%, 40%, 60%, 80%, and 100% methanol containing 0.1% TFA). Reversed-phase LC-MS analysis (10-100% aqueous acetonitrile in 0.1% trifluoroacetic acid, 30-min gradient) revealed that the 60% fraction included both molecules **1** and **2**, and the fraction was dried under reduced pressure. This fraction (60 mg) was then separated by reversed-phase HPLC equipped with an Agilent Polaris C_{18}-A 5 μm (21.2 × 250 mm) column with an isocratic solvent system (50% acetonitrile in water, 0.1% TFA, over 20 min, 8 mL min^{-1}, 1-min fraction collection interval). Compound **1** from the pooled fraction (11+12) (t_R = 25.3 min, 0.2 mg) was partially purified over the Phenomenex Luna C_8 (2) 10 μm (10.0 × 250mm) column with a linear gradient elution (20-80% acetonitrile in water, 0.1% TFA, over 30 min). The combined HPLC fraction (11+12) was subsequently purified by reversed-phase HPLC (Phenomenex Luna C_{18} (2) 10 μm (10.0 × 250mm) column) with a linear gradient elution (20-80% acetonitrile in water, 0.1% TFA, over 30 min) to yield pure compound **2** (t_R = 25.8 min, 1.2 mg). Compound **4** was detected in the 80% aqueous methanol Sep-Pak fraction and was separated over an Agilent Polaris C_{18}-A 5 μm (21.2 × 250 mm) column (Flow rate: 8.0 ml/min; Gradient elution: 10-100% aqueous acetonitrile in 0.1% TFA for 30 min, 1-min fraction collection). HPLC fraction 24 was then separated over the Phenomenex Luna C_{18} (2) 10 μm (10.0 × 250mm) column with 50-100% acetonitrile in

water containing 0.1% TFA over 30 min at a flow rate of 4 ml min^{-1} followed by the subjection to Agilent Polaris 5 Amide-C18 (250 × 10.0 mm) with the same elution system (Flow rate: 4 ml min^{-1}: Purification method: 50-100% acetonitrile in water containing 0.1% TFA over 30 min) to yield pure compound **4** (t_R = 9.43 min, 0.7 mg).

(*E*)-6-(non-1-en-1-yl)-2,3,4,5-tetrahydropyridine (**1**): colorless solid; ^{1}H NMR (CD_3OD, 600 MHz) δ 7.21-7.12 (1H, m, H-8), 6.35 (1H, d, J = 16.0 Hz, H-7), 3.59 (2H, m, H-2), 2.91 (2H, m, H-5), 2.30 (2H, m, H-9), 1.77 (2H, m, H-3), 1.71 (2H, m, H-4), 1.42 (2H, m, H-10), 1.27-1.20 (8H, m, H-11, H-12, H-13, H-14), 0.84 (3H, t, J = 7.0 Hz, H-15); HR-ESI-QTOF-MS $[M+H]^+$ *m/z* 208.2067 (calcd for $C_{14}H_{26}N$, 208.2065).

6-nonyl-2,3,4,5-tetrahydropyridine (**2**): colorless solid; ^{1}H NMR (CD_3OD, 600 MHz) δ 3.53 (2H, t, J = 5.5 Hz, H-2), 2.72 (2H, t, J = 6.1 Hz, H-5), 2.53 (2H, m, H-7), 1.73 (2H, m, H-3), 1.68 (2H, m, H-4), 1.54 (2H, dt, J = 14.6, 6.8 Hz, H-8), 1.28-1.15 (12H, m, H-9, H-10, H-11, H-12, H-13, H-14), 0.83 (3H, t, J = 7.0 Hz, H-15), ^{13}C NMR (CD_3OD, 125 MHz) δ 192.1 (C-6),44.4 (C-2), 37.7 (C-7), 31.6 (C-13), 29.4 (C-5), 28.0-29.0 (C-9, C-10, C-11, C-12), 25.5 (C-8), 22.5 (C-14), 19.2 (C-3), 16.8 (C-4), 14.4 (C-15); HR-ESI-QTOF-MS $[M+H]^+$ *m/z* 210.2224 (calcd for $C_{14}H_{28}N$, 210.2222).

(*R*)-*N*-(4-chlorobutyl)-3-hydroxydecanamide (**4**): colorless solid; ^{1}H NMR (CD_3OD, 600 MHz) δ 3.94 (1H, m, H-3), 3.59 (2H, t, J = 6.5 Hz, H-4′), 3.20 (2H, m, H-1′), 2.27 (2H, m, H-2), 1.78

(2H, m, H-3′), 1.63 (2H, dt, J = 14.3, 7.0 Hz, H-2′), 1.43 (2H, m, H-4), 1.36-1.25 (10H, m, H-5, H-6, H-7, H-8, H-9), 0.90 (3H, t, J = 6.9 Hz, H-10), ^{13}C NMR (CD_3OD, 125 MHz) δ 172.6 (C-1), 68.2 (C-3), 44.1 (C-4′), 43.8 (C-2), 37.9 (C-1′), 36.8 (C-4), 31.8 (C-8), 29.5 (C-3′), 29.4 (C-5 or C-6, C-7), 26.3 (C-2′), 22.6 (C-5 or C-6, C-9), 13.4 (C-10); HR-ESI-QTOF-MS $[M+H]^+$ *m/z* 278.1885 (calcd for $C_{14}H_{29}ClNO_2$, 278.1887).

Determination of absolute configuration of metabolite 4. The absolute configuration of **4** was determined using the modified Mosher's method with *R*- and *S*-α-methoxy-(trifluoromethyl)phenylacetyl chloride (MTPA-Cl) (28). Compound **4** (0.5 mg) was prepared in two vials (0.25 mg), and each sample was dissolved in 250 μL of dried pyridine-d_5 in vials purged with N_2 gas. Dimethylaminopyridine (DMAP) (0.5 mg) was added to both vials followed by the addition of 5 μL of *S*- and *R*-MTPA-Cl solution (2% v/v) at room temperature. After 18 h, the reaction mixtures were dried under reduced pressure. ^{1}H NMR spectra of the Mosher esters (*S*-MTPA ester and *R*-MTPA ester) were collected in methanol-d_4, and the chemical shift differences of the Mosher esters of **4** were calculated in $\Delta\delta_{S-R}$.

Characterization of *Pseudomonas* sp. SWI36. *Pseudomonas* sp. SWI36 and *P. koreensis* inhibitory interactions against *B. cereus* and *F. johnsoniae* were evaluated with a modified spread-patch method. Strains were grown separately for 20 h. One-mL aliquots of cultures of each strain were centrifuged (6000 × *g*, 6 min), resuspended in one ml of the same medium (undiluted cultures), and a 1:100 dilution of *B. cereus* and *F. johnsoniae* was prepared in

the same medium (diluted culture). Nutrient agar plates were spread with 100 μL of either *B. cereus* or *F. johnsoniae* diluted cultures and spotted with 10 μL of the undiluted cultures of *Pseudomonas* sp. SWI36 and *P. koreensis*. Plates were then incubated at 28°C and inspected for zones of inhibition after two days. Crude extract of *Pseudomonas* sp. SWI36 and *Pseudomonas* sp. SWI36 *kecF*::Tn culture in nutrient broth were prepared as above. Extracted materials were analyzed on a LC/MS system consisting of a Thermo Fisher Scientific (Waltham, MA) Q Exactive orbitrap mass spectrometer with an electrospray ionization (ESI) source coupled to a Vanquish UHPLC (Column: Thermo Accucore Vanquish C18 column, 100 × 2.1 mm, 1.5 μm; Flow rate: 0.2 ml min^{-1}; mobile phase composition: H_2O and acetonitrile (ACN) containing 0.1% trifluoroacetic acid (TFA); method: 0-1 min, 10% ACN; 1-4 min, 10-35% ACN; 4-12 min, 35-70% ACN; 12-16 min, 70-98% ACN; 16-20 min hold with 98% ACN; 20-21 min, 98-10% ACN; 21-23 min, 10% ACN). MS1 scans were acquired with positive ionization over a *m/z* range of 188-1275 with settings of 1e6 AGC, 100 ms maximum integration time, and 70k resolution.

Phylogenetic analysis. Genetic regions with homology to the koreenceine biosynthetic cluster were identified by BLAST alignment tools (29) using *P. koreensis* CI12 KecF protein sequence in the NCBI database. All the KecF homologues identified were part of koreenceine-like cluster. Genomes harboring koreenceine-like clusters are listed in Table S1. Protein and nucleotide sequence alignments of *kecF* were performed with MAFFT version 7 (30) and were manually adjusted using as a guide the residues-wise confidence scores generated by GUIDANCE2 (31). Best-fit models of amino acid or nucleotide replacement were selected. Evolutionary analyses were inferred by Maximum Likelihood (ML) methods conducted in

509 MEGA X (32). The *P. koreensis* and *P. mandelii* phylogenomic reconstruction was done by the
510 phylogenetic and molecular evolutionary (PhaME) analysis software (33). PhaME identified
511 SNPs from the core genome alignments, and the phylogenetic relationships were inferred by ML
512 using FastTree. Phylogenetic trees were visualized using interactive tree of life (iTOL) (34).
513
514 **REFERENCES**

515 1. **Berg G**, **Grube M**, **Schloter M**, **Smalla K**. 2014. Unraveling the plant microbiome:
516 looking back and future perspectives. Front Microbiol **5**:148.
517 2. **Bais HP**, **Weir TL**, **Perry LG**, **Gilroy S**, **Vivanco JM**. 2006. The role of root exudates in
518 rhizosphere interactions with plants and other organisms. Annu Rev Plant Biol **57**:233–
519 266.
520 3. **Arshad M**, **Frankenberger WT Jr.** 1998. Plant growth-regulating substances in the
521 rhizosphere: microbial production and functions. Adv Agron **62**:45–151.
522 4. **Handelsman J**, **Stabb EV**. 1996. Biocontrol of soilborne plant pathogens. Plant Cell
523 **8**:1855–1869.
524 5. **Bulgarelli D**, **Schlaeppi K**, **Spaepen S**, **Ver Loren van Themaat E**, **Schulze-Lefert P**.
525 2013. Structure and functions of the bacterial microbiota of plants. Annu Rev Plant Biol
526 **64**:807–838.
527 6. **Lozano GL**, **Bravo JI**, **Garavito Diago MF**, **Park HB**, **Hurley A**, **Peterson SB**, **Stabb**
528 **EV**, **Crawford JM**, **Broderick NA**, **Handelsman J**. 2018. Introducing THOR, a model
529 microbiome for genetic dissection of community behavior. bioRxiv 499715.
530 7. **Valentini M**, **García-Mauriño SM**, **Pérez-Martínez I**, **Santero E**, **Canosa I**, **Lapouge**
531 **K**. 2014. Hierarchical management of carbon sources is regulated similarly by the CbrA/B

systems in *Pseudomonas aeruginosa* and *Pseudomonas putida*. Microbiology **160**:2243–2252.

8. **Nishijyo T**, **Haas D**, **Itoh Y**. 2001. The CbrA-CbrB two-component regulatory system controls the utilization of multiple carbon and nitrogen sources in *Pseudomonas aeruginosa*. Mol Microbiol **40**:917–931.

9. **Vetter J**. 2004. Poison hemlock (*Conium maculatum* L.). Food Chem Toxicol **42**:1373–1382.

10. **Leete E**. 1964. Biosynthesis of the hemlock alkaloids. The incorporation of acetate-1-C^{14} into coniine and conhydrine. J Am Chem Soc **86**:2509–2513.

11. **Hotti H**, **Seppänen-Laakso T**, **Arvas M**, **Teeri TH**, **Rischer H**. 2015. Polyketide synthases from poison hemlock (*Conium maculatum* L.). FEBS J **282**:4141–4156.

12. **Roberts MF**. 1971. The formation of γ-coniceine from 5-ketooctanal by a transaminase of *Conium maculatum*. Phytochemistry **10**:3057–3060.

13. **Roberts MF**. 1981. Enzymic synthesis of γ-coniceine in *Conium maculatum* chloroplasts and mitochondria. Plant Cell Rep **1**:10–13.

14. **Schirmer A**, **Rude MA**, **Li X**, **Popova E**, **del Cardayre SB**. 2010. Microbial biosynthesis of alkanes. Science **329**:559–562.

15. **Blitzke T**, **Porzel A**, **Masaoud M**, **Schmidt J**. 2000. A chlorinated amide and piperidine alkaloids from *Aloe sabaea*. Phytochemistry **55**:979–982.

16. **Abe I**, **Morita H**. 2010. Structure and function of the chalcone synthase superfamily of plant type III polyketide synthases. Nat Prod Rep **27**:809–838.

17. **Chung EJ**, **Lim HK**, **Kim J-C**, **Choi GJ**, **Park EJ**, **Lee MH**, **Chung YR**, **Lee S-W**. 2008. Forest soil metagenome gene cluster involved in antifungal activity expression in

Escherichia coli. Appl Environ Microbiol **74**:723–730.

18. **Davis E**, **Sloan T**, **Aurelius K**, **Barbour A**, **Bodey E**, **Clark B**, **Dennis C**, **Drown R**, **Fleming M**, **Humbert A**, **Glasgo E**, **Kerns T**, **Lingro K**, **McMillin M**, **Meyer A**, **Pope B**, **Stalevicz A**, **Steffen B**, **Steindl A**, **Williams C**, **Wimberley C**, **Zenas R**, **Butela K**, **Wildschutte H**. 2017. Antibiotic discovery throughout the Small World Initiative: a molecular strategy to identify biosynthetic gene clusters involved in antagonistic activity. Microbiologyopen **6**:e00435.

19. **Garrido-Sanz D**, **Meier-Kolthoff JP**, **Göker M**, **Martín M**, **Rivilla R**, **Redondo-Nieto M**. 2016. Genomic and genetic diversity within the *Pseudomonas fluorescens* complex. PLoS ONE **11**:e0150183.

20. **Thomashow LS**, **Weller DM**. 1988. Role of a phenazine antibiotic from *Pseudomonas fluorescens* in biological control of *Gaeumannomyces graminis* var. tritici. J Bacteriol **170**:3499–3508.

21. **Haney CH**, **Samuel BS**, **Bush J**, **Ausubel FM**. 2015. Associations with rhizosphere bacteria can confer an adaptive advantage to plants. Nat Plants **1**:15051.

22. **Martins dos Santos VAP**, **Timmis KN**, **Tümmler B**, **Weinel C**. 2004. Genomic features of *Pseudomonas putida* strain KT2440, pp. 77–112. *In Pseudomonas*. Springer US, Boston, MA.

23. **Bis DM**, **Ban YH**, **James ED**, **Alqahtani N**, **Viswanathan R**, **Lane AL**. 2015. Characterization of the nocardiopsin biosynthetic gene cluster reveals similarities to and differences from the rapamycin and FK-506 pathways. ChemBioChem **16**:990–997.

24. **Peng H**, **Wei E**, **Wang J**, **Zhang Y**, **Cheng L**, **Ma H**, **Deng Z**, **Qu X**. 2016. Deciphering piperidine formation in polyketide-derived indolizidines reveals a thioester reduction,

578 transamination, and unusual imine reduction process. ACS Chem Biol **11**:3278–3283.

579 25. **Reynolds T**. 2005. Hemlock alkaloids from Socrates to poison aloes. Phytochemistry
580 **66**:1399–1406.

581 26. **Hoagland DR**, **Arnon DI**. 1950. The water-culture method for growing plants without
582 soil. Calif Agric Exp Stat Circ **347**:1–32.

583 27. **Sivakumar R**, **Ranjani J**, **Vishnu US**, **Jayashree S**, **Lozano GL**, **Miles J**, **Broderick N**,
584 **Guan C**, **Gunasekaran P**, **Handelsman J**, **Rajendhran J**. 2018. Evaluation of InSeq to
585 identify genes essential for *Pseudomonas aeruginosa* PGPR2 corn root colonization.
586 bioRxiv 377168.

587 28. **Hoye TR**, **Jeffrey CS**, **Shao F**. 2007. Mosher ester analysis for the determination of
588 absolute configuration of stereogenic (chiral) carbinol carbons. Nat Protoc **2**:2451–2458.

589 29. **Altschul SF**, **Gish W**, **Miller W**, **Myers EW**, **Lipman DJ**. 1990. Basic local alignment
590 search tool. J Mol Biol **215**:403–410.

591 30. **Katoh K**, **Standley DM**. 2013. MAFFT multiple sequence alignment software version 7:
592 improvements in performance and usability. Mol Biol Evol **30**:772–780.

593 31. **Sela I**, **Ashkenazy H**, **Katoh K**, **Pupko T**. 2015. GUIDANCE2: accurate detection of
594 unreliable alignment regions accounting for the uncertainty of multiple parameters.
595 Nucleic Acids Res **43**:W7–14.

596 32. **Kumar S**, **Stecher G**, **Li M**, **Knyaz C**, **Tamura K**. 2018. MEGA X: Molecular
597 evolutionary genetics analysis across computing platforms. Mol Biol Evol **35**:1547–1549.

598 33. **Ahmed SA**, **Lo C-C**, **Li P-E**, **Davenport KW**, **Chain PSG**. 2015. From raw reads to
599 trees: Whole genome SNP phylogenetics across the tree of life. bioRxiv 032250.

600 34. **Letunic I**, **Bork P**. 2016. Interactive tree of life (iTOL) v3: an online tool for the display

and annotation of phylogenetic and other trees. Nucleic Acids Res **44**:W242–5.

FIGURES AND TABLES

FIG 1. Koreenceine biosynthetic locus and the predicted function of each gene. Black arrows indicate locations of the transposons of the mutants identified.

FIG 2. Extracted ion chromatograms of koreenceine A-D for wild type and *kecA-K* deletion mutant.

FIG 3. Structural characterization of koreenceines A) Chemical structures of compounds **1**-**4.** B) Key COSY and HMBC NMR correlations of compounds. C) $\Delta\delta_{S-R}$ in ppm for the MTPA esters of compound **4**.

FIG 4. Predicted biosynthetic pathway for γ-coniceine in plants and proposed biosynthetic pathway for koreenceine B in *P. koreensis*. Similar functions are color coded to highlight the similarity between both routes in plants and koreenceine biosynthetic locus.

FIG 5. Phylogenetic analysis of the koreenceine biosynthetic locus and its distribution across bacteria. A) Maximum likelihood phylogenetic tree estimated from the amino acid sequence of KecF, and the corresponding structure of the koreenceine-like gene cluster present in each clade. B) Schematic representation of the koreenceine-like biosynthetic locus and its genomic context from several *Pseudomonas* spp. from clade A and clade B. Genes conserved in all genomes from *P. mandelii* and *P. koreensis* are in dark gray, meanwhile variable or unique genes are in gray. Genes that likely experienced horizontal gene transfer events are in yellow. C) Comparison of

647 the phylogenies of *kecF* genes and their associated *Pseudomonas* genomes belonging to Clade A
648 *kecF* homologues. Both phylogenies correspond to maximum likelihood analyses of the
649 nucleotide sequence of the genes or the core genome. The dotted lines connect the cluster with
650 its corresponding *Pseudomonas* genome.
651
652 **Table 1.** *P. koreensis* mutants identified in the genetic screen with loss of inhibitory activity
653 against *F. johnsoniae*.
654
655 **Table 2.** Primers used in this study.
656
657 **FIG S1.** Genetic validation of the role of koreenceine gene cluster in inhibition of *F. johnsoniae*
658 and other Bacteroidetes. Several Bacteroidetes members of the soybean rhizosphere population
659 when grown alone, with *P. koreensis* wild type, or *P. koreensis* CI12 *kecA-K*::*tet.* ND, not
660 detected.
661
662 **FIG S2.** Development of a minimal medium to mimic *P. koreensis* inhibition against *F.*
663 *johnsoniae*. A) *P. koreensis* and *F. johnsoniae* in co-culture in a define medium with glucose,
664 mannitol or pyruvate as a carbon sources with or without amino acid mixture. B) *P. koreensis*
665 and *F. johnsoniae* in co-culture in a defined minimal media with or without amino acid mixture,
666 or a single amino acid, or N-methyl-DL-aspartate (Asp*) a non-hydrolysable analog of aspartate.
667
668 **FIG S3.** HRESIQTOFMS spectral data of compounds **1- 4**
669

FIG S4. NMR spectra of compound **1**

FIG S5. NMR spectra of compound **2**

FIG S6. (A-D) NMR spectra of compound **4** (E) ^{1}H NMR spectra comparison of *S*-MTPA (blue) and *R*-MTPA (maroon) of compound **4** (F) gCOSY NMR spectrum of *S*-MTPA of compound **4** (G) gCOSY NMR spectrum of *R*-MTPA of compound **4**

FIG S7. Tandem MS spectra of compounds **1**-**4**

FIG S8. Predicted uncharacterized halogenation reaction and oxidation/reduction of γ-coniceine and koreenceine C.

FIG S9. Activity profile of *P. koreensis* and *Pseudomonas* sp. SWI36 against *B. cereus* and *F. johnsoniae*.

FIG S10. Extracted ion chromatograms of koreenceine C for *Pseudomonas* sp SWI36 wild type and *kecF*::*Tn* mutant.

Table S1. Bacterial genomes containing gene clusters with high similarity to the koreenceine cluster.

FIG 1.

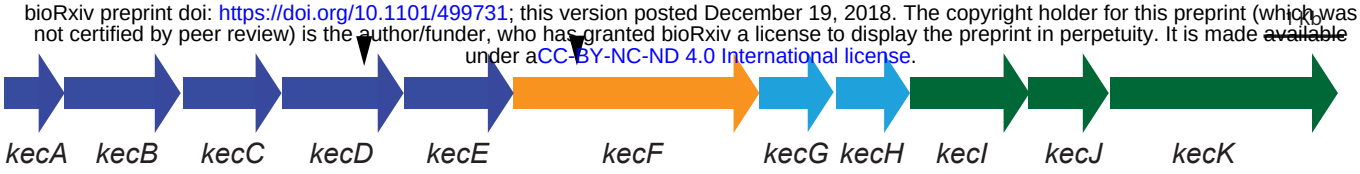

Polyketide synthase genes

kecA	Acyl-carrier protein
kecB - kecD	β-ketoacyl synthase
kecC - kecE	Thiolase-like domain

Polyketide accessory genes

kecG - kecH	Ketoreductase
kecM	NAD(P)H reductase

Transaminase

kecF	Pyridoxalphosphate-dependent aminotransferase / Acyl-ACP reductase

Others

kecI - kecJ	Hypothetical protein
kecK	Transporter

FIG 2.

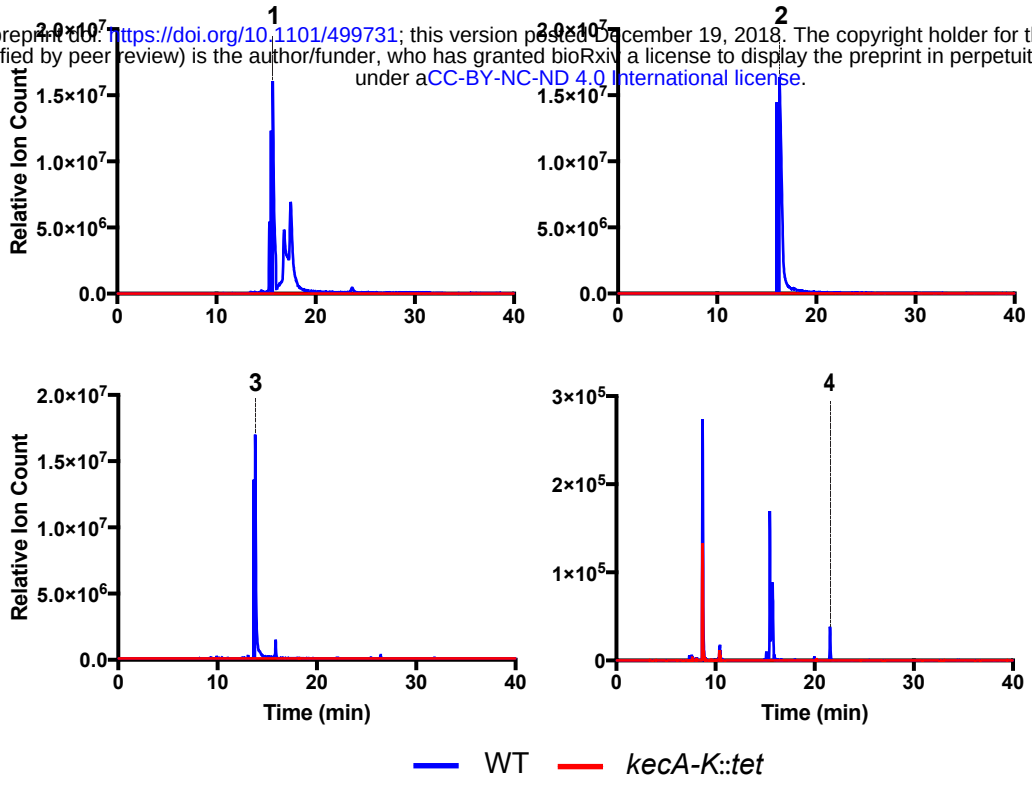

FIG 3.

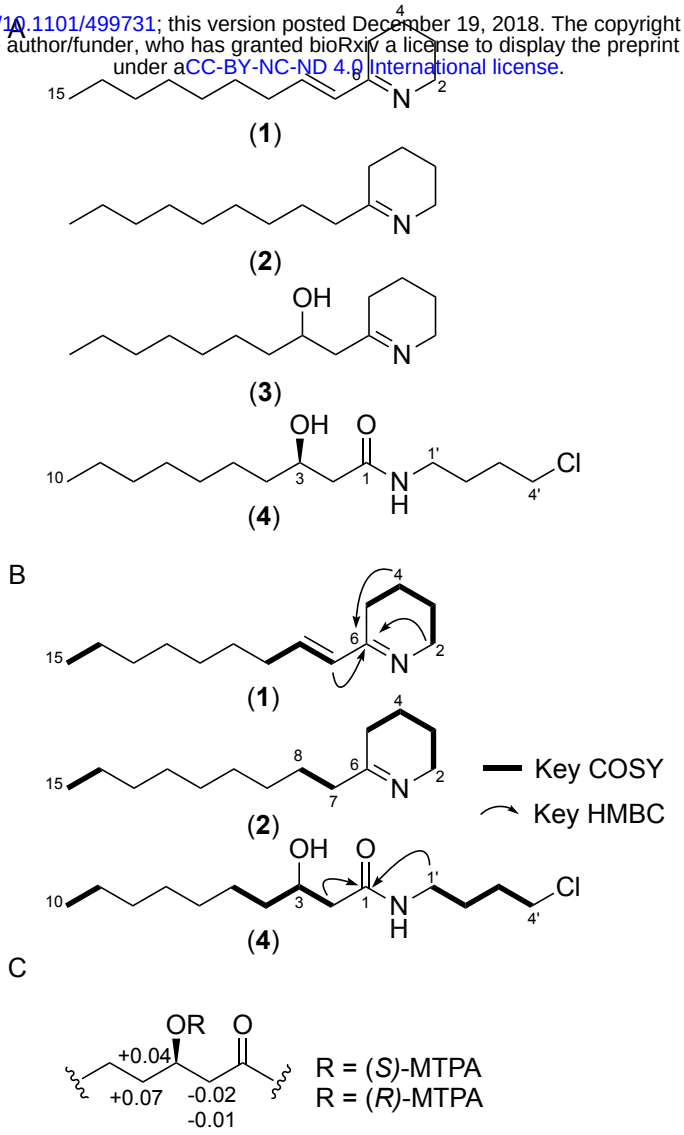

FIG 4.

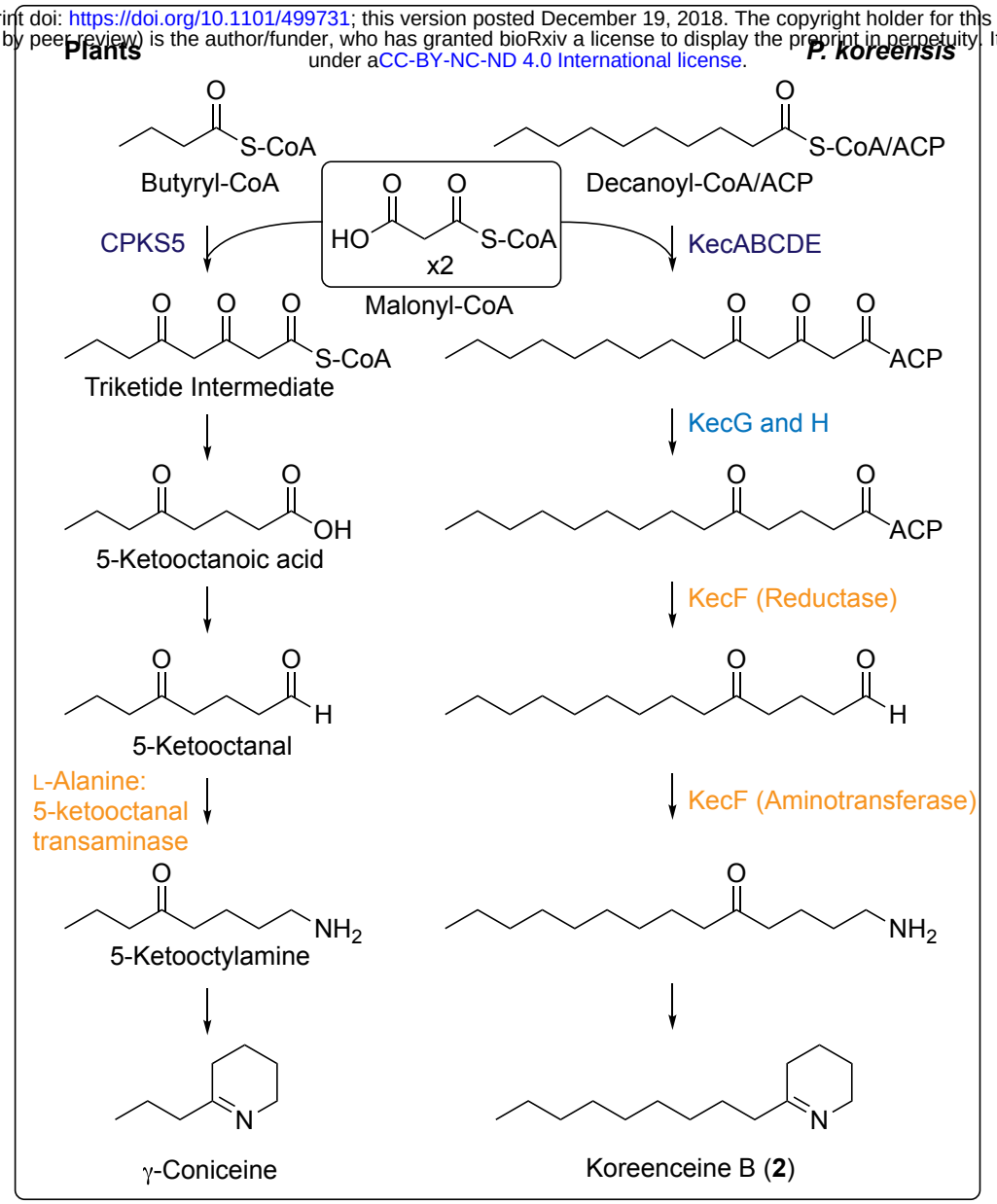

FIG 5.

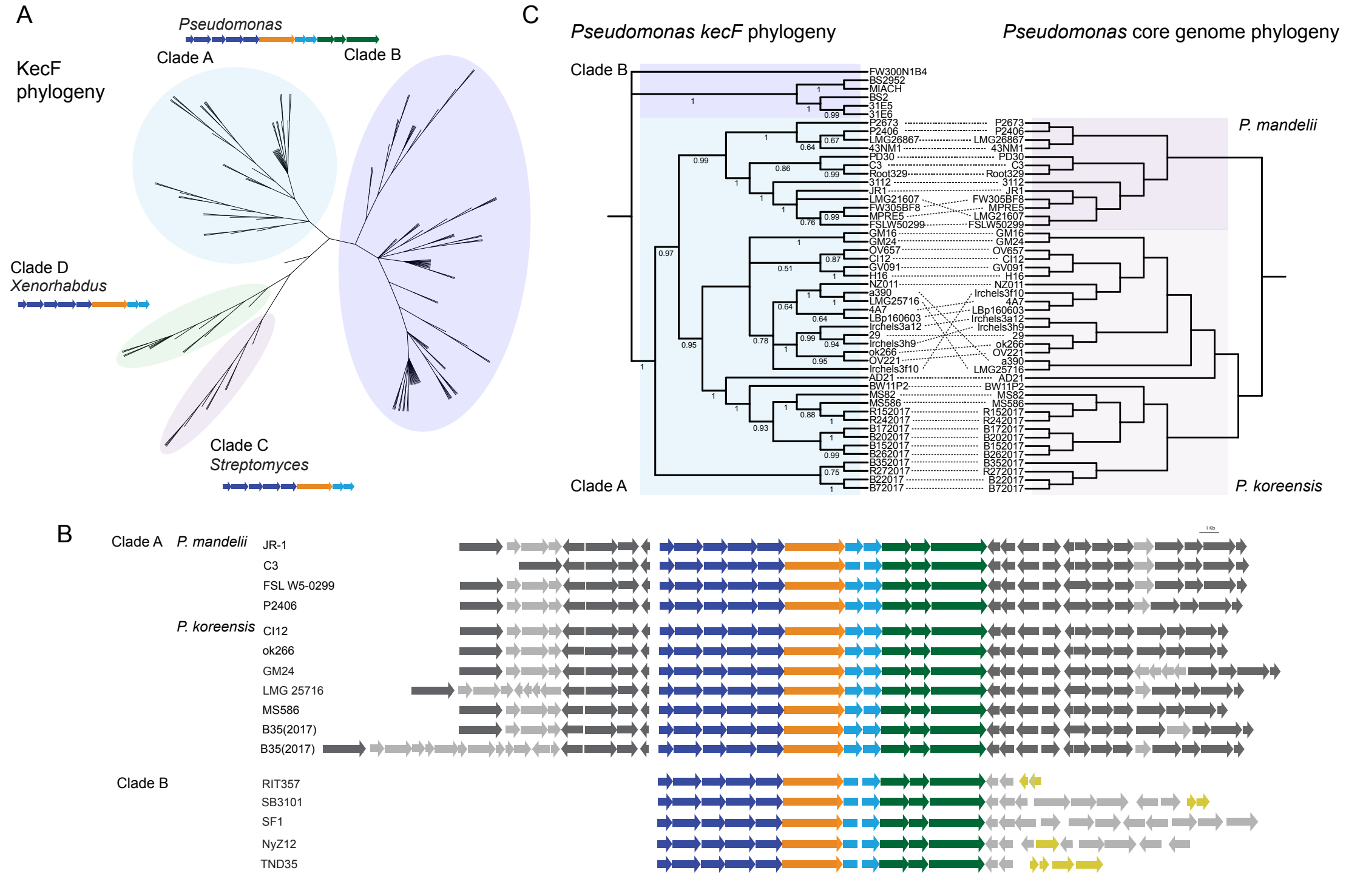
A
Pseudomonas
Clade A
Clade B
KecF
phylogeny
Clade D
Xenorhabdus
Clade C
Streptomyces
C
Pseudomonas kecF phylogeny
Pseudomonas core genome phylogeny
Clade B
Clade A
P. mandelii
P. koreensis
FW300N1B4
BS2952
MIACH
BS2
31E5
31E6
P2673
P2406
LMG26867
43NM1
PD30
C3
Root329
3112
JR1
LMG21607
FW305BF8
MPRE5
FSLW50299
GM16
GM24
QV657
CI12
GV091
H16
NZ011
a390
LMG25716
4A7
LBp160603
Irchels3a12
29
Irchels3h9
ok266
OV221
Irchels3f10
AD21
BW11P2
MS82
MS586
R152017
R242017
B172017
B202017
B152017
B262017
B352017
R272017
B22017
B72017
B
Clade A
P. mandelii
JR-1
C3
FSL W5-0299
P2406
P. koreensis
CI12
ok266
GM24
LMG 25716
MS586
B35(2017)
B35(2017)
Clade B
RIT357
SB3101
SF1
NyZ12
TND35

Table 1.

Mutant	ID	Predicted Function	Class
1	OOH83074	Pyridoxalphosphate dependent aminotransferase	Secondary metabolites production
2	OOH83072	3-oxoacyl-ACP synthase	Secondary metabolites production
3, 4	OOH76777	Two-component sensor histidine kinase CbrA	Cell signaling and transcription regulation
5, 6	OOH78126	CysB family transcriptional regulator	Cell signaling and transcription regulation
7	OOH78405	Multi-sensor hybrid histidine kinase	Cell signaling and transcription regulation
8	OOH81884	Outer membrane protein assembly factor BamC	Cell surface
9	OOH77437	Peptidoglycan-associated lipoprotein	Cell surface
10	OOH75718	Phospholipid/glycerol acyltransferase	Cell surface
11	OOH75539	Acetylglutamate kinase	Metabolism
12	OOH81129	Methylcitrate synthase	Metabolism
13	OOH76758	Ketol-acid reductoisomerase	Metabolism
14	OOH80977	Succinyl-CoA synthetase subunit alpha	Metabolism
15	OOH81130	2-methylisocitrate dehydratase	Metabolism
16[a]	OOH76781	3-methyl-2-oxobutanoate hydroxymethyltransferase	Metabolism
	OOH76782	Pantoate-beta-alanine ligase	Metabolism

[a] Transposon insertion in the promoter, 5' region, of an operon conformed for these two genes

Table 2.

Name	Sequence
GenPATseq1	CTTGGATGCCCGAGGCATAG
GenPATseq2	CTGTACAAAAAAACAGTCATAACAAGCCATG
AR1A	GGCCACGCGTCGACTAGTACNNNNNNNNNNGTAAT
AR1B	GGCCACGCGTCGACTAGTACNNNNNNNNNNGATGC
AR2	GGCCACGCGTCGACTAGTAC
mutSGCA_For	CACCCGCAAGCCTGCAATAGACGGAC
mutSGCA_Rev	CCTGTCGTCTCAGGAAAGGTGCGGTACCTTCTATCTCCCTATATGTCGTGAC
mutSGCB_For	GTCACGACATATAGGGAGATAGAAGGTACCGCACCTTTCCTGAGACGACAGG
mutSGCB_Rev	GCACCTGACATTCGTCTATCCGATC
TetA_For	CACCGGTACCTCCTCCAAGCCAGTTACCTCGG
TetA_Rev	GGTACCTGCTCAGGTCGCAGACGTTTTG
pJN105Mob_For	TAGGCGCGCCTGTGGTCAAGCTCGTGGGC
pJN105Mob_Rev	CACCGGCGCGCCCAATTCGTTCAAGCCGAGATCGGC

FIG S1.

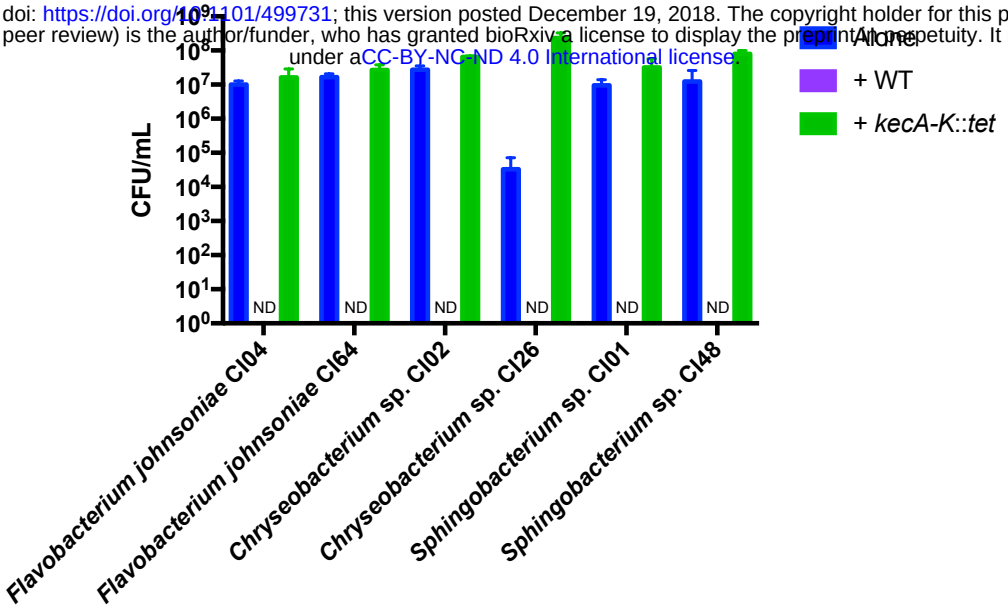

FIG S2.

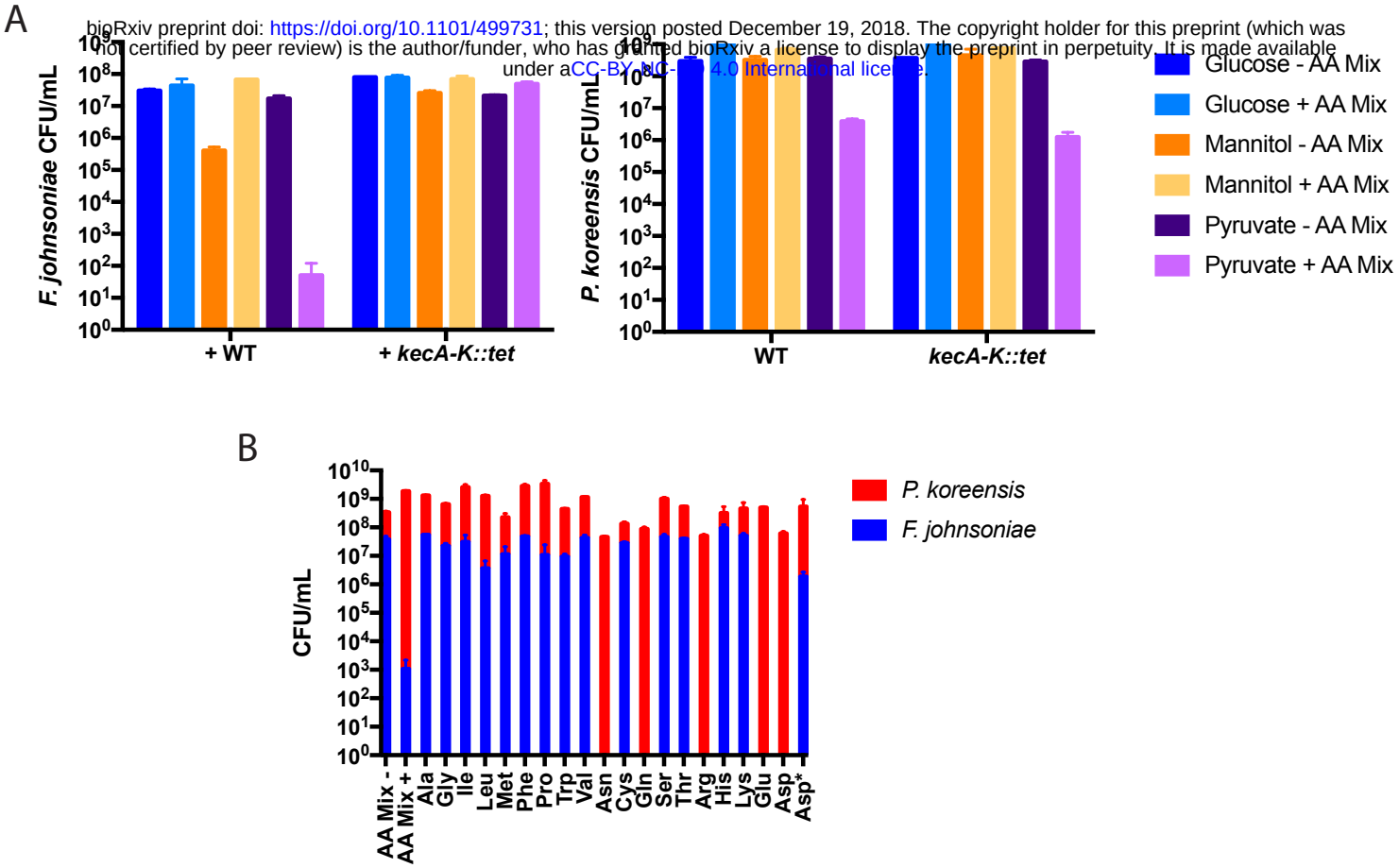

FIG S3.

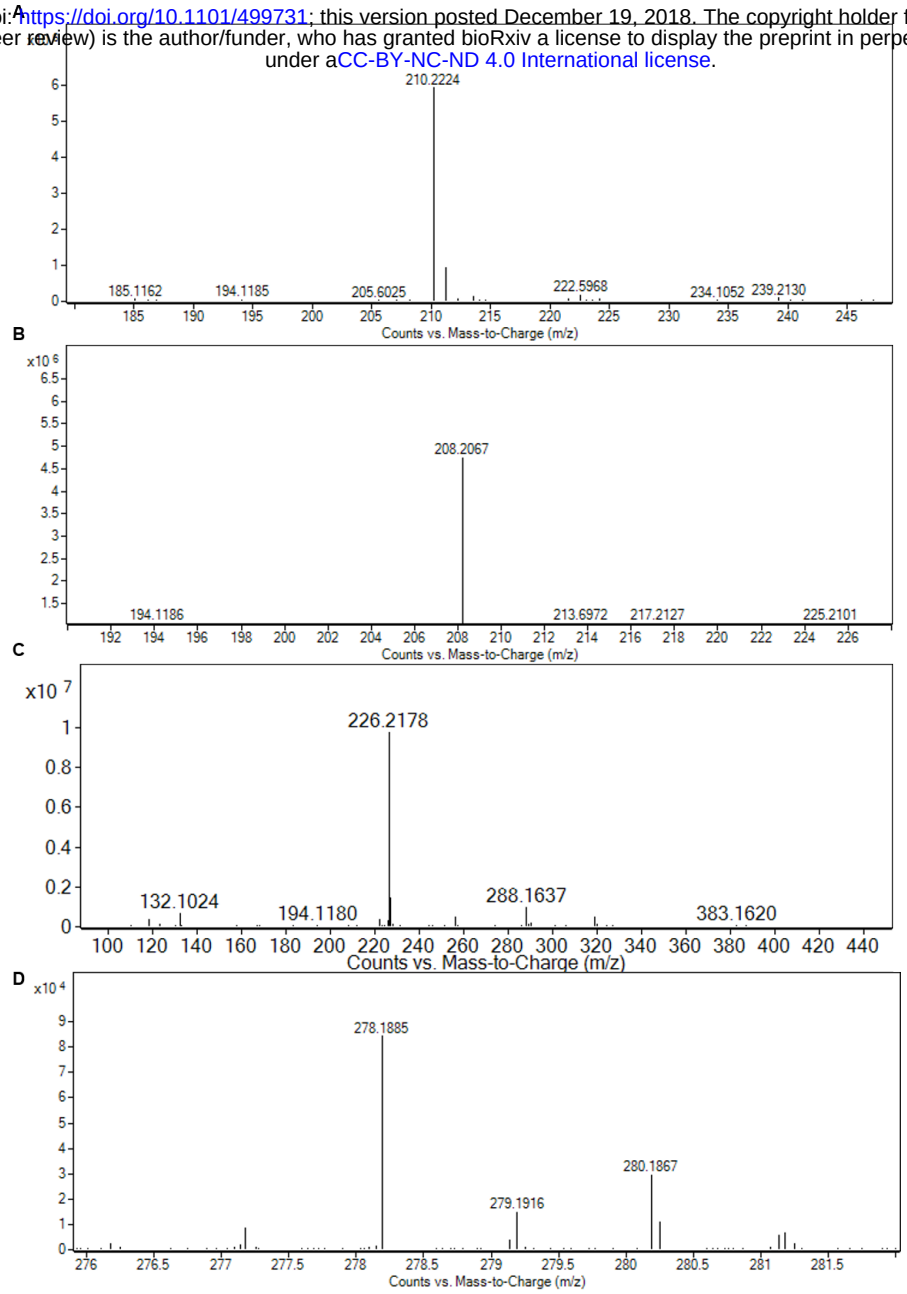

FIG S4.

A

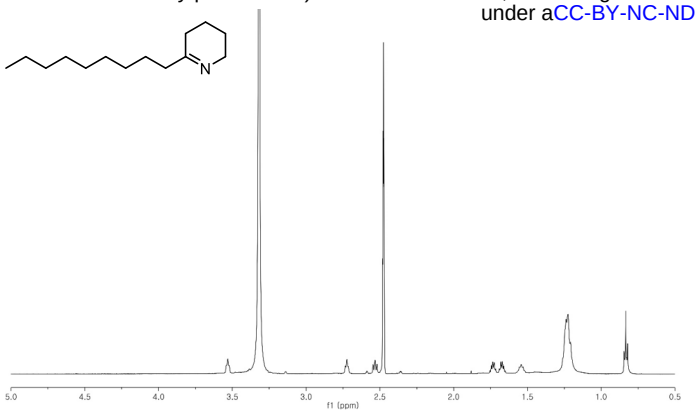

B

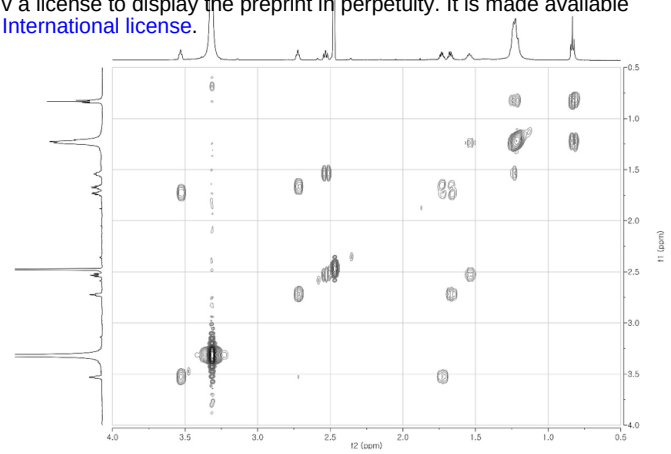

C

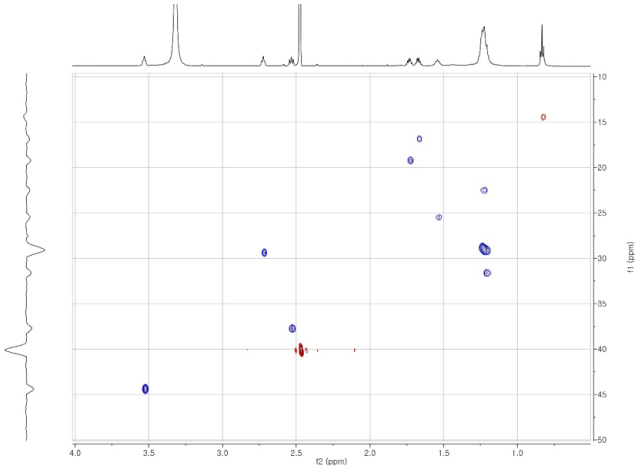

D

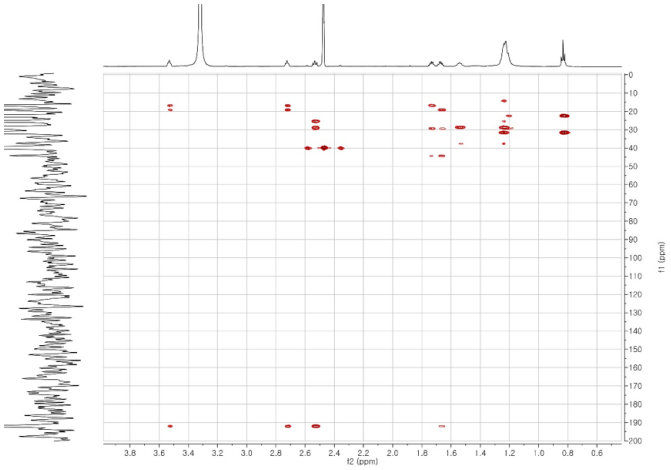

FIG S5.

A

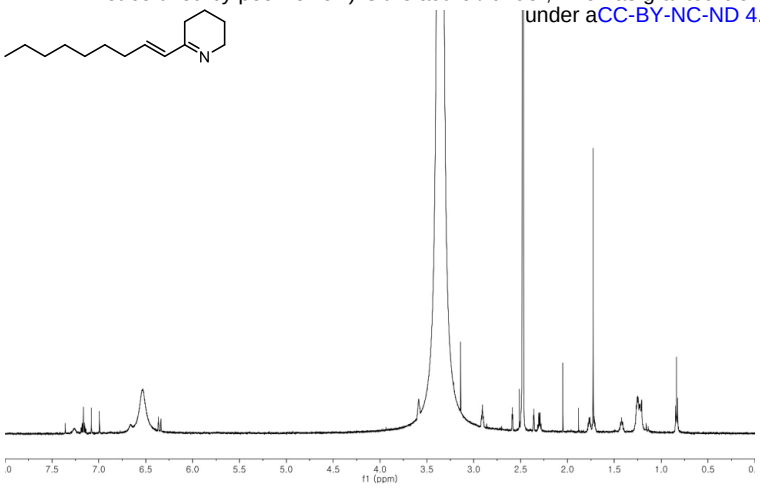

B

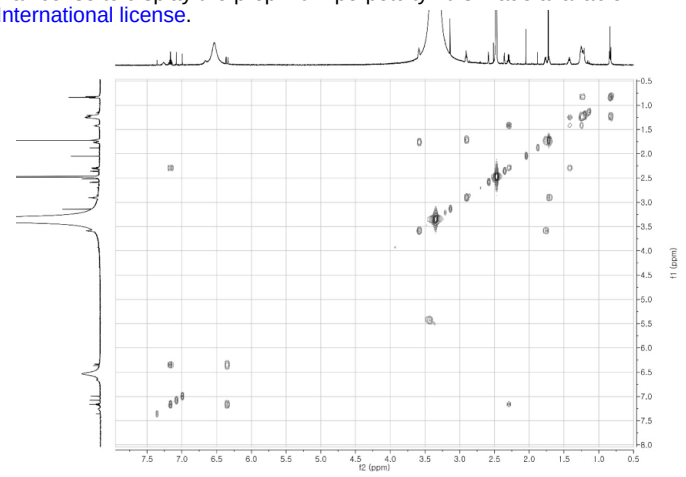

FIG S6.

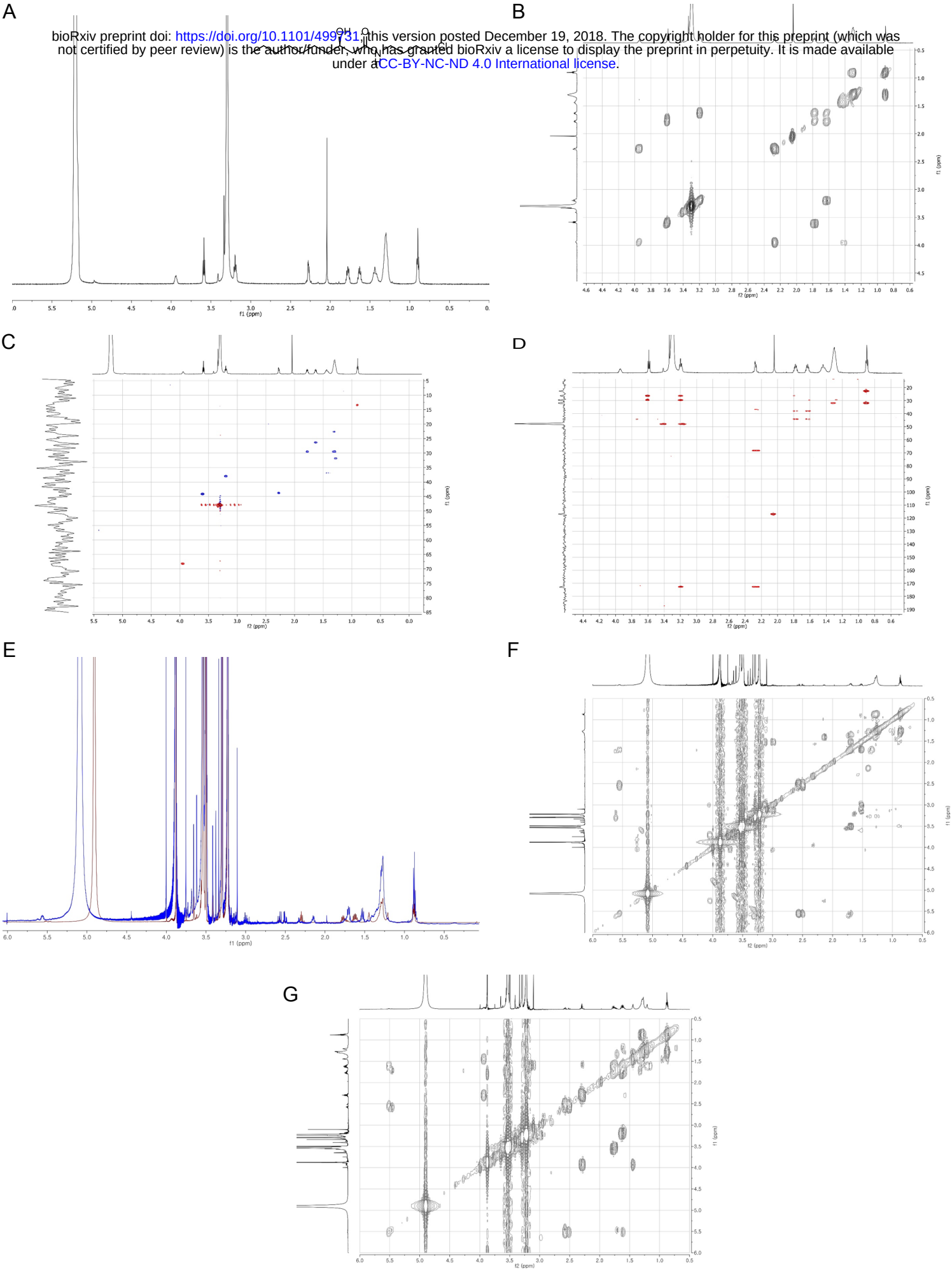

FIG S7.

Compound **1**

Observed MS/MS fragmentation pattern of koreenceine A

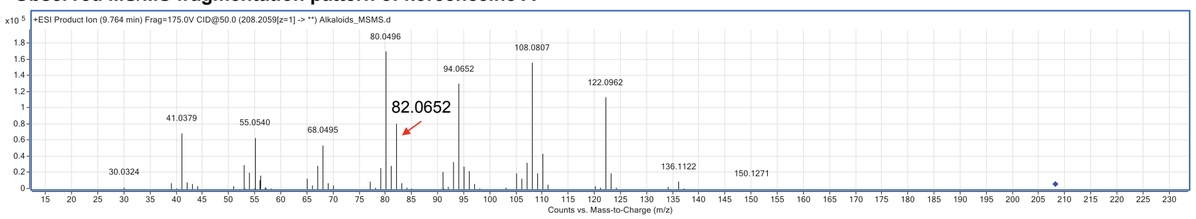

Calculated MS/MS fragmentation pattern of koreenceine A

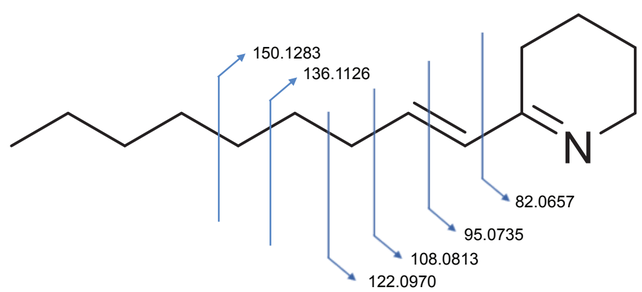

Compound **2**

Observed MS/MS fragmentation pattern of koreenceine B

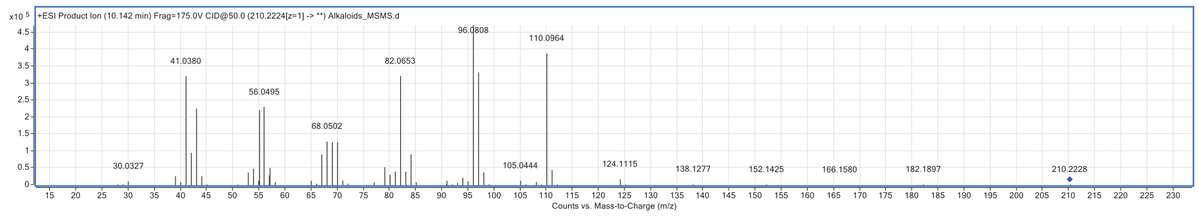

Calculated MS/MS fragmentation pattern of koreenceine B

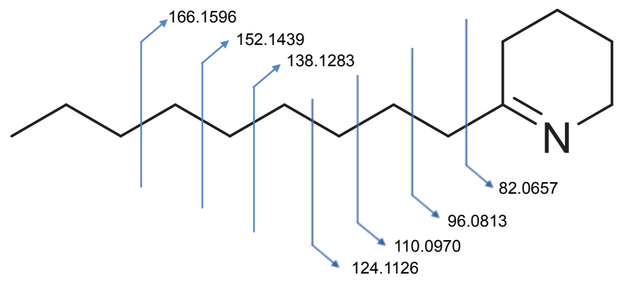

Compound **3**

Observed MS/MS fragmentation pattern of koreenceine C

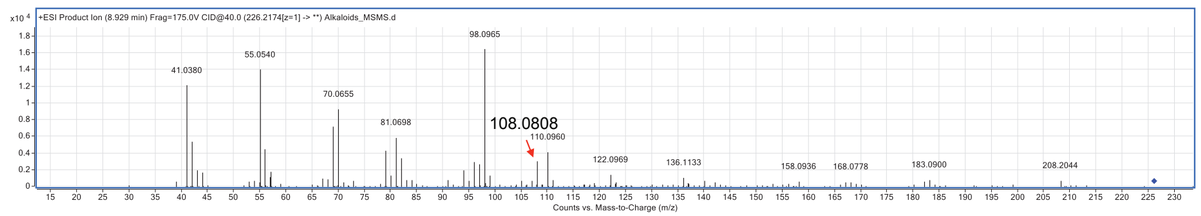

Calculated MS/MS fragmentation pattern of koreenceine C

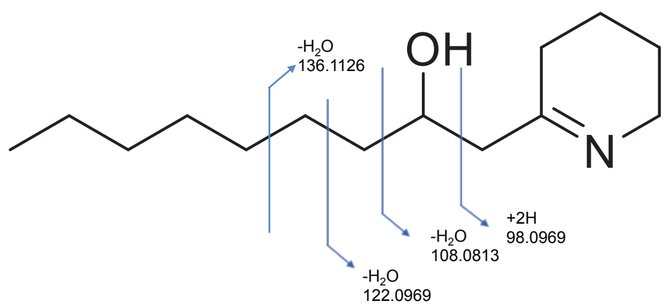

Compound **4**

Observed MS/MS fragmentation pattern of koreenceine D

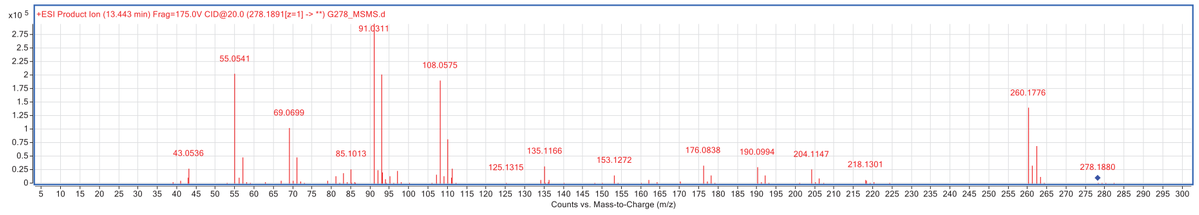

Calculated MS/MS fragmentation pattern of koreenceine D

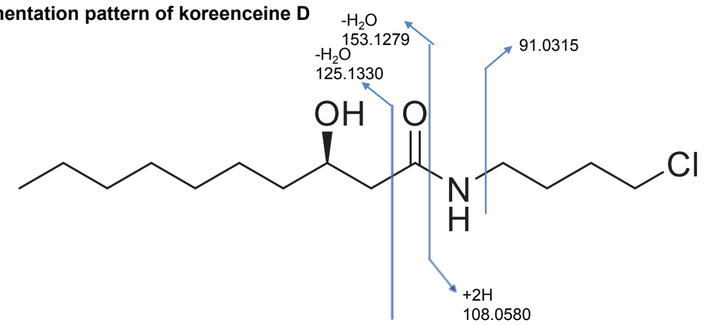

FIG S8.

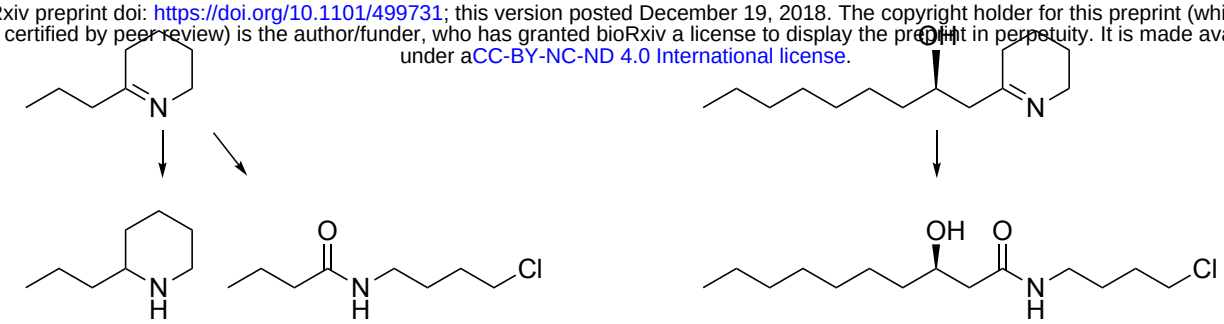

FIG S9.

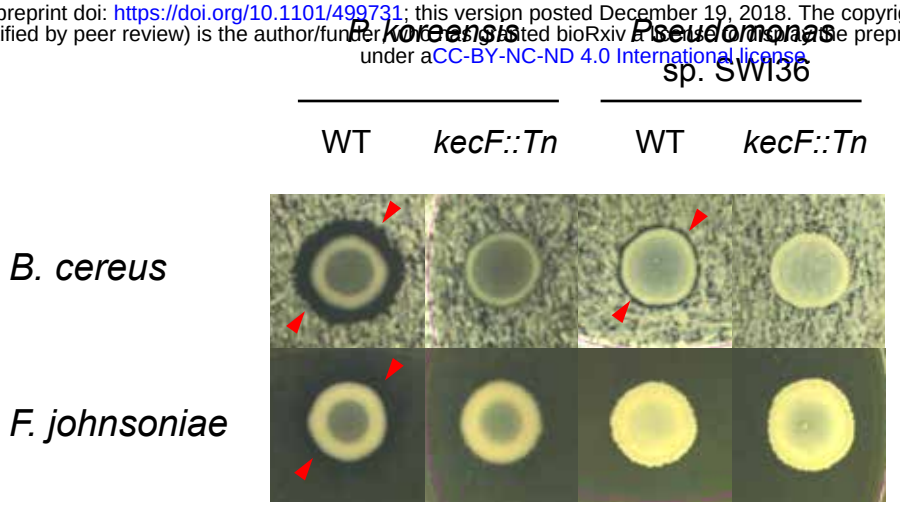

FIG S10.

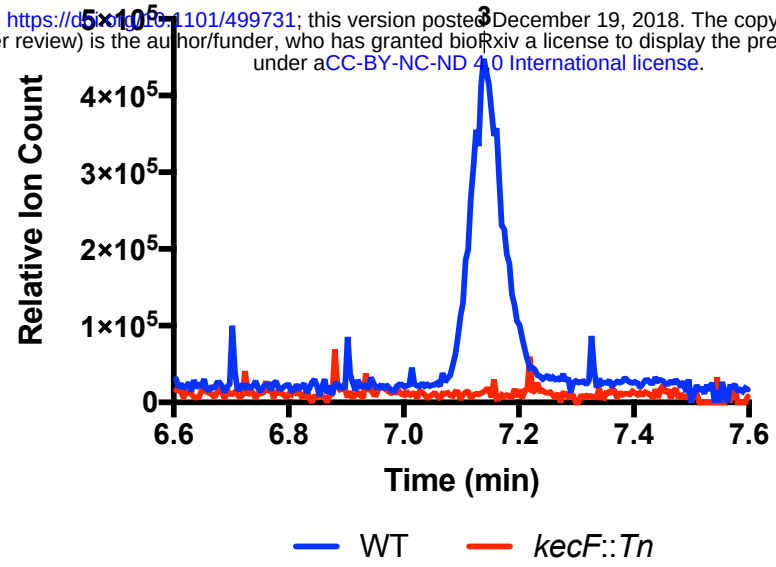

Table S1.

Name	Abbreviation	GenBank assembly accession	Koreenceine-like cluster clade
[*Flavobacterium*] sp. 29	29	GCA_002754355	A
Pseudomonas asplenii 4A7	4A7	GCA_002891515	A
Pseudomonas baetica a390	a390	GCA_003031005	A
Pseudomonas baetica LMG 25716	LMG25716	GCA_002813455	A
Pseudomonas fluorescens NZ011	NZ011	GCA_000276585	A
Pseudomonas fluorescens BW11P2	BW11P2	GCA_001679645	A
Pseudomonas fluorescens C3	C3	GCA_000967955	A
Pseudomonas fluorescens H16	H16	GCA_000802985	A
Pseudomonas fluorescens MS82	MS82	GCA_003055645	A
Pseudomonas jessenii LBp-160603	LBp160603	GCA_003205375	A
Pseudomonas koreensis CI12	CI12	GCA_002003425	A
Pseudomonas mandelii JR-1	JR1	GCA_000257545	A
Pseudomonas mandelii PD30	PD30	GCA_000690555	A
Pseudomonas mandelii LMG 21607	LMG21607	GCA_900106065	A
Pseudomonas prosekii LMG 26867	LMG26867	GCA_900105155	A
Pseudomonas prosekii P2406	P2406	GCA_003122265	A
Pseudomonas prosekii P2673	P2673	GCA_003122305	A
Pseudomonas sp. 31-12	3112	GCA_003151075	A
Pseudomonas sp. 43NM1	43NM1	GCA_002836905	A
Pseudomonas sp. AD21	AD21	GCA_002878485	A
Pseudomonas sp. B15(2017)	B152017	GCA_002113215	A
Pseudomonas sp. B17(2017)	B172017	GCA_002113765	A
Pseudomonas sp. B2(2017)	B22017	GCA_002113685	A
Pseudomonas sp. B20(2017)	B202017	GCA_002113125	A
Pseudomonas sp. B26(2017)	B262017	GCA_002113045	A
Pseudomonas sp. B35(2017)	B352017	GCA_002113645	A
Pseudomonas sp. B7(2017)	B72017	GCA_002112745	A
Pseudomonas sp. FSL W5-0299	FSLW50299	GCA_002005125	A
Pseudomonas sp. FW305-BF8	FW305BF8	GCA_002883215	A
Pseudomonas sp. GM16	GM16	GCA_000282155	A
Pseudomonas sp. GM24	GM24	GCA_000282235	A
Pseudomonas sp. GV091	GV091	GCA_003053805	A
Pseudomonas sp. Irchel s3a12	Irchels3a12	GCA_900187485	A
Pseudomonas sp. Irchel s3f10	Irchels3f10	GCA_900187515	A
Pseudomonas sp. Irchel s3h9	Irchels3h9	GCA_900187475	A

Pseudomonas sp. MPR-E5	MPRE5	GCA_002883015	A
Pseudomonas sp. MS586	MS586	GCA_001594225	A
Pseudomonas sp. Ok266	ok266	GCA_900110195	A
Pseudomonas sp. OV221	OV221	GCA_003391605	A
Pseudomonas sp. OV657	OV657	GCA_003386585	A
Pseudomonas sp. R15(2017)	R152017	GCA_002112685	A
Pseudomonas sp. R23(2017)	R232017	GCA_002112575	A
Pseudomonas sp. R24(2017)	R242017	GCA_002113465	A
Pseudomonas sp. R27(2017)	R272017	GCA_002113445	A
Pseudomonas sp. Root329	Root329	GCA_001424925	A
Pseudomonas fluorescens BS2	BS2	GCA_000308175	B
Pseudomonas fluorescens AHK-1	AHK1	GCA_003363095	B
Pseudomonas fluorescens FW300-N1B4	FW300N1B4	GCA_001625455	B
Pseudomonas hunanensis P11	P11	GCA_002910975	B
Pseudomonas marginalis BS2952	BS2952	GCA_900105325	B
Pseudomonas monteilii SB3078	SB3078	GCA_000510285	B
Pseudomonas monteilii SB3101	SB3101	GCA_000510325	B
Pseudomonas monteilii MO2	MO2	GCA_001571445	B
Pseudomonas plecoglossicida DJ-1	DJ1	GCA_002307455	B
Pseudomonas plecoglossicida MR134	MR134	GCA_002864885	B
Pseudomonas plecoglossicida MR135	MR135	GCA_002864795	B
Pseudomonas plecoglossicida MR170	MR170	GCA_002864845	B
Pseudomonas plecoglossicida MR69	MR69	GCA_002864775	B
Pseudomonas plecoglossicida MR70	MR70	GCA_002864905	B
Pseudomonas plecoglossicida MR83	MR83	GCA_002864865	B
Pseudomonas plecoglossicida NyZ12	NyZ12	GCA_000831585	B
Pseudomonas plecoglossicida TND35	TND35	GCA_000764405	B
Pseudomonas putida B6-2	B62	GCA_000226035	B
Pseudomonas putida BIRD-1	BIRD1	GCA_000183645	B
Pseudomonas putida F1	F1	GCA_000016865	B
Pseudomonas putida HB3267	HB3267	GCA_000325725	B
Pseudomonas putida JB	JB	GCA_001767335	B
Pseudomonas putida KT2440	KT2440	GCA_000007565	B
Pseudomonas putida LS46	LS46	GCA_000294445	B
Pseudomonas putida ND6	ND6	GCA_000264665	B
Pseudomonas putida S12	S12	GCA_000495455	B
Pseudomonas putida SJTE-1	SJTE1	GCA_000271965	B
Pseudomonas putida Idaho	Idaho	GCA_000226475	B
Pseudomonas putida CA-3	CA3	GCA_002810225	B

Pseudomonas putida DPA1	DPA1	GCA_002891885	B
Pseudomonas putida strain DZ-C18	DZC18	GCA_002094795	B
Pseudomonas putida FDAARGOS_409	FDAARGOS409	GCA_002554535	B
Pseudomonas putida H	H	GCA_001077495	B
Pseudomonas putida HB13667	HB13667	GCA_001306495	B
Pseudomonas putida INSali382	INSali382	GCA_001653615	B
Pseudomonas putida JLR11	JLR11	GCA_001183585	B
Pseudomonas putida KCJK7911	KCJK7911	GCA_003053335	B
Pseudomonas putida N1R	N1R	GCA_900156185	B
Pseudomonas putida P1	P1	GCA_001865225	B
Pseudomonas putida PD1	PD1	GCA_000799625	B
Pseudomonas putida SF1	SF1	GCA_001027965	B
Pseudomonas putida UV4	UV4	GCA_002165695	B
Pseudomonas putida UV4/95	UV495	GCA_002165665	B
Pseudomonas putida TRO1	TRO1	GCA_000367825	B
Pseudomonas taiwanensis SJ9	SJ9	GCA_000500605	B
Pseudomonas sp. 22 E 5	22E5	GCA_900004705	B
Pseudomonas sp. 2822-17	282217	GCA_002742485	B
Pseudomonas sp. 2995-1	29951	GCA_002742505	B
Pseudomonas sp. 31 E 5	31E5	GCA_900005815	B
Pseudomonas sp. 31 E 6	31E6	GCA_900005935	B
Pseudomonas sp. B12(2017)	B122017	GCA_002113785	B
Pseudomonas sp. B13(2017)	B132017	GCA_002113245	B
Pseudomonas sp. B14(2017)	B142017	GCA_002113255	B
Pseudomonas sp. B22(2017)	B222017	GCA_002113105	B
Pseudomonas sp. B23(2017)	B232017	GCA_002113725	B
Pseudomonas sp. B24(2017)	B242017	GCA_002113085	B
Pseudomonas sp. B28(2017)	B282017	GCA_002113025	B
Pseudomonas sp. B4(2017)	B42017	GCA_002113565	B
Pseudomonas sp. B8(2017)	B82017	GCA_002113575	B
Pseudomonas sp. C5pp	C5pp	GCA_000814065	B
Pseudomonas sp. CC6-YY-74	CC6YY74	GCA_002025205	B
Pseudomonas sp. FFUP_PS_41	FFUPPS41	GCA_002858645	B
Pseudomonas sp. FW305-E2	FW305E2	GCA_002901725	B
Pseudomonas sp. GTC 16473	GTC16473	GCA_001753855	B
Pseudomonas sp. GTC 16482	GTC16482	GCA_001319995	B
Pseudomonas sp. Irchel 3H9	Irchel3H9	GCA_900187495	B
Pseudomonas sp. JY-Q	JYQ	GCA_001655295	B
Pseudomonas sp. Leaf58	Leaf58	GCA_001422615	B

Pseudomonas sp. LG1E9	LG1E9	GCA_003290225	B
Pseudomonas sp. MIACH	MIACH	GCA_001269925	B
Pseudomonas sp. MR 02	MR02	GCA_002797475	B
Pseudomonas sp. NBRC 111118	NBRC111118	GCA_001320085	B
Pseudomonas sp. NBRC 111121	NBRC111121	GCA_001320165	B
Pseudomonas sp. NBRC 111125	NBRC111125	GCA_001320295	B
Pseudomonas sp. NBRC 111136	NBRC111136	GCA_001320745	B
Pseudomonas sp. NBRC 111139	NBRC111139	GCA_001753955	B
Pseudomonas sp. OV577	OV577	GCA_003386595	B
Pseudomonas sp. P21	p21	GCA_001642705	B
Pseudomonas sp. PGPPP2	PGPPP2	GCA_002255825	B
Pseudomonas sp. RIT357	RIT357	GCA_000632245	B
Pseudomonas sp. RW405	RW405	GCA_003184135	B
Pseudomonas sp. SID14000	SID14000	GCA_002165135	B
Pseudomonas sp. SMT-1	SMT1	GCA_003204195	B
Pseudomonas sp. SWI36	SWI36	GCA_002948105	B
Pseudomonas sp. XWY-1	XWY1	GCA_002953115	B
Streptomyces albulus CCRC 11814	CCRC11814	GCA_000403765	C
Streptomyces albulus NK660	NK660	GCA_000695235	C
Streptomyces albulus PD-1	SaPD1	GCA_000504065	C
Streptomyces albus ZpM	ZpM	GCA_000963515	C
Streptomyces diastatochromogenes NRRL B-1698	NRRLB1698	GCA_001418405	C
Streptomyces noursei ATCC 11455	ATCC11455	GCA_001704275	C
Streptomyces yunnanensis CGMCC 4.3555	CGMCC43555	GCA_900142595	C
Streptomyces sp. MspMP-M5	MspMPM5	GCA_000373585	C
Streptomyces sp. NRRL F-4489	NRRLF4489	GCA_001509485	C
Xenorhabdus bovienii CS03	CS031	GCA_000973125	D
Xenorhabdus bovienii CS03	CS032	GCA_000973125	D
Xenorhabdus bovienii feltiae Florida	Florida	GCA_000736675	D
Xenorhabdus bovienii feltiae France	France	GCA_000736655	D
Xenorhabdus bovienii feltiae Moldova	Moldova	GCA_000736595	D
Xenorhabdus bovienii intermedium	intermedium	GCA_000736615	D
Xenorhabdus bovienii kraussei	kraussei	GCA_00073669	D
Xenorhabdus bovienii kraussei Quebec	Quebec	GCA_000736555	D
Xenorhabdus bovienii oregonense	oregonense	GCA_000736535	D
Xenorhabdus bovienii puntauvense	puntauvense	GCA_000736635	D
Xenorhabdus khoisanae MCB sp. ICMP 17674	ICMP17674	GCA_001037465	D
Xenorhabdus poinarii G6	G6	GCA_000968175	D
Xenorhabdus sp. NBAII XenSa04	XenSa04	GCA_000798625	D

Uncultured bacterium	pEAF66	EU099626	